

**Determination of an empirical correlation for the mass transfer coefficients of
pharmaceutical powders in a Fluid Bed Dryer**

By

Magaly Arocho Serrano

A thesis submitted in partial fulfillment
of the requirements for the degree of

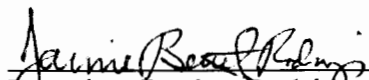
MASTER OF SCIENCE

In

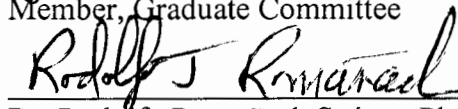
Chemical Engineering

UNIVERSITY OF PUERTO RICO
MAYAGÜEZ CAMPUS
2004

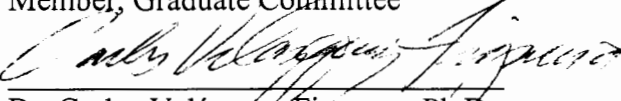
Approved by


Dr. Jaime Benítez Rodríguez, Ph.D.
Member, Graduate Committee

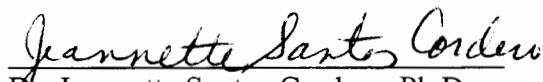
April 30, 2004
Date


Dr. Rodolfo Romañach Suárez, Ph.D.
Member, Graduate Committee

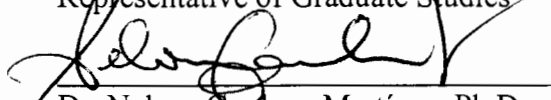
April 30, 2004
Date


Dr. Carlos Velázquez Figueroa, Ph.D.
President, Graduate Committee

April 28, 2004
Date


Dr. Jeannette Santos Cordero, Ph.D.
Representative of Graduate Studies

April 28, 2004
Date


Dr. Nelson Cardona Martínez, Ph.D.
Chairperson of the Department

April 30, 2004
Date

ABSTRACT

The pharmaceutical industry has four basic operations to produce tablets: mixing, drying, milling, and tablet pressing. Fluidized bed drying of the pharmaceutical powders is one of the most efficient methods, which is finding ever-growing applications in diverse industries, especially in the pharmaceutical and the food industries. However, one of the problems that exist in the pharmaceutical industry is to determine when the formulation reaches the desired moisture content. This final value can be either determined with a Loss on Drying (LOD) technique or estimated using a model of the process. To obtain this model, it is necessary to know the parameters that control drying process as well as the characteristics of the granulation used in this stage. Unfortunately the modeling of drying is still uncertain. The objective of this research was to determine an empirical correlation for the mass transfer coefficient ($k_g a$) of pharmaceutical powders in a Fluid Bed Dryer (FBD) which will then be used along with fundamental models to predict moisture content. Granulations of blends consisting of lactose monohydrate and pregelatinized starch combined with distilled water were dried and samples were withdrawn at different intervals of time to generate drying curves. These curves were divided in two regions, the constant and the falling rate periods. Correlations based on dimensionless numbers such as Reynolds, Schmidt, and Sherwood were developed. Predicted values were compared to values obtained from Loss on Drying (LOD). Good correlation was obtained between predicted values of $k_g a$ with the experimental ones. Additionally, an average residual of 0.18 % was obtained. It was found that the air flow velocity is the most significant factor in the drying curve behavior. Other phenomena

such as bed porosity and changing the composition of the granulation seem not to affect the prediction of moisture content (MC) for the granulation used. The study indicates that prediction of MC curves of some pharmaceutical powders in a FBD can be achieved by establishing a correlation of $k_g a$ based just on air flow and temperature.

RESUMEN

La industria farmacéutica tiene cuatro operaciones básicas para producir tabletas llamada: mezclado, secado, molido y compresión de tableta. Secado en lecho fluidizado en polvos farmacéutica es uno de los métodos modernos de secado eficiente y se ha encontrado un crecimiento de aplicaciones en diversas industrias, especialmente en la industria farmacéutica y de alimento. Sin embargo, uno de los problemas que existe en la industria farmacéutica es en el término para predecir cuando la formulación alcanza un contenido de humedad requerido. Este valor final puede ser determinado con la técnica de pérdida por secado (LOD) estimando un modelo de proceso utilizado. Para obtener este modelo es necesario conocer los parámetros que controlan el proceso de secado como también las características de la granulación usada en esta etapa. Desafortunadamente, los modelos en secado aun son inciertos. El objetivo de esta investigación es determinar el coeficiente de transferencia de masa ($k_g a$) en polvos farmacéuticos en un secador de lecho fluidizado (FBD) el cual va hacer usado a lo largo con modelos fundamentales para predecir el contenido de humedad. Las granulaciones consisten de dos polvos, lactosa monohidratada y almidón pregelatinizado, combinados con agua destilada los cuales fueron secados y las muestras fueron tomados a diferentes intervalos de tiempo para generar las curvas de secado. Las curvas fueron divididas en dos periodos, secado constante y de decaimiento. Las correlaciones fueron desarrolladas basadas en los números adimensionales tales como Reynolds, Schmidt, y Sherwood. Los valores predichos fueron comparados con los valores obtenidos por la utilización de la técnica de pérdida por secado (LOD). Se obtuvo un buen acuerdo entre los valores predichos de $k_g a$

y los experimentales. Además, se obtuvo un promedio residual de 0.18 %. Se encontró que el flujo de aire es el factor que más afecta en el comportamiento de la curva de secado. Otros fenómenos como la porosidad del lecho y la variación en la composición de la granulación al parecer no afectan la predicción del contenido de humedad. La predicción de las curvas del contenido de humedad de algunos polvos farmacéuticos en un secador de lecho fluidizado pueden ser determinadas por las correlaciones de $k_g a$ en términos de velocidad y temperatura del aire.

Master's Thesis of Magaly Arocho Serrano
University of Puerto Rico, Mayagüez Campus

Copyright @ 2004 by Magaly Arocho Serrano. All rights reserved. Printed in the United States of America. Except as permitted under the United States Copyright Act of 1976, no part of this publication may be reproduced or distributed in any form or by any means, or stored in a data base or retrieved system, without the prior written permission of the publisher.

This thesis is dedicated primarily to God for his unconditional love and strength that gave me to be able to leave in victory, to my family (Arocho-Serrano) and my boyfriend (Eng Omar Viera), for their continuous support. Special mention to my mother Felícita Serrano, my father, Héctor Arocho and my sisters, Cely and Damarys, my bothers in law, Rafy and Erick and specially to my nephew, Raphdiel, for his smile and songs.

ACKNOWLEDGEMENTS

Special mention and profound gratitude to the people who made this work possible in one way or another: God, my family, Eng Omar Viera (my love), Diana Siberio (my best friends who inspired me to continue in graduate school), Eunice Olivero for her sincere friendship and songs, Dr. Carlos Velazquez, Dr Jaime Benitez, Dr. Rodolfo Romañach, Federico Padrón (PE), Dr. Nelson Cardona (for recommending me to the GLOBE Program), Chemical Engineering Department professors and secretaries (Wally, Nora, Sylvia, Audrey, Sulma, Jorge, and others), to people who works in the workshop specially Angel L. Zapata with his kids, students of GUEST k-12, specially María Rodriguez and Zaida Pagán for their friendship, Ricardo Camacho for believing in me and helping me to growth in areas like Biology, Geology, CBL, sensors and others, Dr. Juan Lopez Garriga (SONW director), Lisa Betancourt and Rosaly (SONWEC Staff), Elsa Toro, Melva and Ritsdeliz (housemates), undergraduates students (Jorge Rivera, Osvaldo Rodriguez, José Cotto, Sully, Brenda Muñiz (piece design), Michelle Vázquez, Milagros Torres, Maritza Muñiz, Meralis and María Teresa Román), Graduates students between 1999-2004. Special mention to Luis Murillo (El Muri), Reynaldo Colón, Lissette Lopez, Ernesto Borrero, Johnny Maury, Luis Obregón (El Firme), Juan Carlos Pulido (El Pelao), Lorena Padró (my lunch partner), Jessica Román, Elizabeth Rivera, Cenilda Ramírez, María Gabriela, Andres (El bogotano), Alba, Eder Vicuña, Monica and Angelines Castro, Caryvette Mejías and Chavely Nieves, for their support and friendship, Antonio Rivera for his prayer and support (music's teacher), NSF (fellowship) and INDUNIV (research funding), Mutchler and Colorcon (laboratory materials); and thanks to Iglesia Evangélica Independiente “Faro de Luz” for their prayers and for helping me in the weekends at Mayagüez.

TABLE OF CONTENT

Chapter I: Introduction	1
I.1 Justification	1
I.2 Objectives	3
Chapter II: Background and Literature Review	4
II.1 Definitions of fluidization	4
II.2 Fluidized drying	4
II.3 Drying curve	5
II.4 Drying models	9
II.5 Mass transfer in Fluid Bed Dryers	14
II.5.1 Mass transfer coefficients	14
Chapter III: Materials and Methods	19
III.1 Materials for drying experiments	19
III.1.2 Equipment for drying curves experiments	20
III.1.3 Methodology for drying curves experiments	21
III.1.3.1 Powder weighing	21
III.1.3.2 Wet granulation preparation	22
III.1.3.3 Fluid bed drying	23
III.1.3.4 LOD moisture analyzer	24
Chapter IV: Sample Calculations	24
IV.1 Drying curves	24
IV.2 Mass transfer coefficients	26
IV.2.1 Constant rate region	28
IV.2.2 Falling rate region	30
IV.3 Developing the empirical correlation	32
IV.4 Prediction of moisture content	38
Chapter V: Results and Discussion	40
V.1 Experimental design	40
V.2 The empirical correlation of the mass transfer coefficient	43

V.3 Prediction of moisture content	53
V.4 Varying composition experiments	57
Chapter VI: Conclusions and Recommendations	65
VI.1 Conclusions	65
VI.2 Recommendation	68
Literature Cited	69
Appendix	71
A. Results of $k_g a$ prediction	72
B. Polymath output to determine the parameters for the empirical correlation	73
C. Prediction of MC for falling rate period (AF1)	76
D. Prediction of MC for constant rate period (AF2)	79
E. Prediction of MC for falling rate period (AF2)	82

LIST OF TABLES

Table III.1. List of ingredients for pharmaceutical granulation	19
Table III.2. Operating conditions used at the FBD	23
Table IV.1. Experimental results of MC and statistical analysis for AF=60 m ³ /hr and T=60 °C	25
Table IV.2. Average data of temperature for the operating conditions of AF=60 m ³ /hr and T=60 °C	27
Table IV.3: Results of k_{ga} for the constant rate period for operating conditions of AF=60 m ³ /hr and T=60 °C	30
Table IV.4. Results of k_{ga} for the falling rate period for operating conditions of AF=60 m ³ /hr, and T=60 °C	31
Table IV.5. Results of Sc , Re and Sh numbers for AF=60 m ³ /hr and T=60 °C in the falling rate period	36
Table IV.6. Results of \overline{Sc} , \overline{Re} and \overline{Sh} numbers for AF1	37
Table IV.7. Results of parameters of the empirical correlations for AF 1 and AF 2	38
Table V.1. Experimental design variables	40
Table V.2. Results of empirical correlation parameters and statistic analysis for AF 1 and AF 2	50
Table A.1. Results of prediction of k_{ga} for the constant rate period for AF1	72
Table A.2. Results of prediction of k_{ga} for the falling rate period for AF1	72
Table A.3. Results of prediction of k_{ga} for the constant rate period for AF2	72
Table A.4. Results of prediction of k_{ga} for the falling rate period for AF2	73

LIST OF FIGURES

Figure II.1. Schematic diagram of the drying process in a particle	6
Figure II.2. Diagram of drying curves, where A-B is the preheating stage, B-C is the constant rate period, C-D is the falling rate period and D-E is the diffusion stage adopted by Lipták.	7
Figure II.3. Diagram of drying rate zones	8
Figure III.1. Schematic of Fluid Bed Dryer and control panel	20
Figure IV.1. Drying curve for operating conditions of $AF=60 \text{ m}^3/\text{hr}$ and $T=60^\circ\text{C}$	26
Figure IV.2. Graphical procedure to determine the critical MC	27
Figure IV.3. Diagram of the FBD bottom to establish the diameter for k_{ga} correlations	33
Figure IV.4. Experimental values of density of water vs temperature	34
Figure V.1. Drying curves for $AF=40, 60$ and $80 \text{ m}^3/\text{hr}$ at $T=60^\circ\text{C}$	42
Figure V.2. Drying curves for $AF=40, 50, 60, 70$ and $80 \text{ m}^3/\text{hr}$ at $T=60^\circ\text{C}$	43
Figure V.3. Experimental mass transfer coefficient values for the constant rate period of AF 1	44
Figure V.4. Experimental mass transfer coefficient values for the falling rate period of AF 1	45
Figure V.5. Re number as a function of air velocity for the constant rate period	47
Figure V.6. Re number as a function of air velocity for the falling rate period	47
Figure V.7. Sh number as a function of air velocity for the constant rate period	48
Figure V.8. Sh number as a function of air velocity for the falling rate period	48
Figure V.9. Sc number as a function of air velocity for the constant rate period	49
Figure V.10. Sc number as a function of air velocity for the falling rate period	49
Figure V.11. Comparison of experimental and predicted k_{ga} for the constant rate period (AF1)	51
Figure V.12. Comparison of experimental and predicted k_{ga} for the falling rate period (AF1)	52
Figure V.13. Comparison of experimental and predicted k_{ga} for the constant rate period (AF2)	52

Figure V.14. Comparison of experimental and predicted k_{ga} for the falling rate period (AF2)	53
Figure V.15. Moisture content prediction for the constant rate period at AF=40 m ³ /hr and T=60 °C	54
Figure V.16. Moisture content prediction for the constant rate period at AF=40 m ³ /hr and T=80 °C	54
Figure V.17. Moisture content prediction for the constant rate period at AF=50 m ³ /hr and T=60 °C	55
Figure V.18. Moisture content prediction for the constant rate period at AF=50 m ³ /hr and T=80 °C	55
Figure V.19. Moisture content prediction for the constant rate period at AF=60 m ³ /hr and T=60 °C	56
Figure V.20. Moisture content prediction for the constant rate period at AF=60 m ³ /hr and T=80 °C	56
Figure V.21. Moisture content prediction for the constant rate period at AF=70 m ³ /hr and T=60 °C	57
Figure V.22. Moisture content prediction for the falling rate period of the varying composition experiments at AF=60 m ³ /hr and T=80 °C	58
Figure V.23. Moisture content prediction for the constant rate period of the varying composition experiments at AF=40 m ³ /hr and T=80 °C	58
Figure V.24. Moisture content prediction for the falling rate period of the varying composition experiments at AF 40=m ³ /hr and T=80 °C	59
Figure V.25. Moisture content prediction for the constant rate period of the varying composition experiments at AF=80 m ³ /hr and T=80 °C	59
FigureV.26. Moisture content prediction for the falling rate period of the varying Composition experiments at AF=80 m ³ /hr and T=80 °C	60
Figure V.32. Particle size distribution for granulation 1.	61
Figure V.32. Particle size distribution for granulation 2.	61
Figure V.29. Moisture content prediction for the constant rate period of the varying composition experiments at AF=80 m ³ /hr and T=60 °C (Formulation3)	63

Figure V.30. Moisture content prediction for the constant rate period of the varying composition experiments at AF=60 m ³ /hr and T=60 °C (Formulation3) using correlations AF1 and AF2	63
Figure V.31. Moisture content prediction for the falling rate period of the varying composition experiments at AF=60 m ³ /hr and T=60 °C (Formulation3) using correlations AF1 and AF2	64
Figure V.32. Particle size distribution for granulation 3.	64
Figure C.1. Diagram of moisture content for falling rate period for AF 50 m ³ /hr and T=80 °C	76
Figure C.2. Diagram of moisture content for falling rate period for AF 50 m ³ /hr and T=60 °C	76
Figure C.3. Diagram of moisture content for falling rate period for AF 60 m ³ /hr and T=80 °C (AF1)	77
Figure C.4. Diagram of moisture content for falling rate period for AF 60 m ³ /hr and T=60 °C (AF1)	77
Figure C.5. Diagram of moisture content for falling rate period for AF 40 m ³ /hr and T=80 °C	78
Figure C.6. Diagram of moisture content for falling rate period for AF 40 m ³ /hr and T=60 °C	78
Figure D.1. Diagram of moisture content for constant rate period for AF 60 m ³ /hr and T=80 °C (AF2)	79
Figure D.2. Diagram of moisture content for constant rate period for AF 60 m ³ /hr and T=60 °C (AF2)	79
Figure D.3. Diagram of moisture content for constant rate period for AF 80 m ³ /hr and T=80 °C	80
Figure D.4. Diagram of moisture content for constant rate period for AF 80 m ³ /hr and T=60 °C	80
Figure D.5. Diagram of moisture content for constant rate period for AF 70 m ³ /hr and T=80 °C	81
Figure E.1. Diagram of moisture content for falling rate period for AF 70 m ³ /hr and T=80 °C	81

Figure E.2. Diagram of moisture content for falling rate period for AF 70 m ³ /hr and T=60 °C	82
Figure E.3. Diagram of moisture content for falling rate period for AF 80 m ³ /hr and T=60 °C	82
Figure E.4. Diagram of moisture content for falling rate period for AF 80 m ³ /hr and T=80 °C	83
Figure E.5. Diagram of moisture content for falling rate period for AF 60 m ³ /hr and T=80 °C (AF2)	83
Figure E.6. Diagram of moisture content for falling rate period for AF 60 m ³ /hr and T=60 °C (AF2)	84

CHAPTER I: INTRODUCTION

I.1 Justification

The pharmaceutical industry has four basic operations to produce tablets, namely mixing, drying, milling, and tablet pressing. The most important operation is drying, since dried products are more stable than moist ones, and the growth of mold and bacteria decreases with lower-moisture content. In addition, drying represents around eighty percent of the total industrial energy consumption (Alden *et. al.* (1988))

Moreover, the moisture content (MC) in pharmaceutical powders affects the mechanical characteristics of tablets. Tablets with low or high MC usually exhibit low mechanical strength. Thus, they could easily be destroyed during packaging, transportation, and home use. This means that there is an optimum residual humidity that produces the strongest mechanical strength in the tablet.

There are many types of drying equipment to achieve the desired MC. These include tray, continuous belt, tumble, spray dryers, fluid bed, rotary steam-tube dryers and others. The simplest dryer is a tray dryer where material to be dried is placed on trays contained in an oven-like enclosure (Kneule (1966)).

The use of a particular drying equipment depends on the characteristics of the powders such as MC and particle size distribution. Fluid Bed Dryers (FBDs) are used to dry loose granular solids and are characterized by a large exchange area between the particles and the gas, and thus, by high heat and mass transfer coefficients. Hence, they provide uniform wet masses for drying, high drying rate, and short drying time. Fluid bed

technology has been widely used in the pharmaceutical industry for applications such as agglomeration, air suspension coating, rotary pelletization, and powder and solution layering.

The monitoring of the MC of product inside the dryer has been traditionally a problem that has affected the efficacy of dryer control methods. In the past, the lack of a good reliable method for direct sensing of a product's MC inside dryers has driven industries to the use of MC surrogates such as exit vapor, product temperature, and air temperature. The development of models for predicting theoretical MC has significantly improved dryer control using only temperature sensors (Robinson (1992)).

Theoretical models and empirical correlations exist to predict the MC of the product (Alden *et. al.* (1988) and Robinson (1992)). However, they do not consider the $k_g a$ factor. Mass transfer in a drying process results from the evaporation rate, which is evaluated using $k_g a$ (Treybal (1978) and Bennett *et. al.* (1982)). Up to now, a formal study has not been developed, where the MC in the FBD for pharmaceutical powders are predicted using $k_g a$.

The significance of this investigation is to provide a correlation to predict the final MC of pharmaceutical powders without having to withdrawing a large number of samples during the drying process. Its development would provide a cost reduction due to the manner of measuring MC using just a predictive correlation. Therefore, the improvement of models to predict MC is of great importance in the processing of pharmaceutical powders and for the improvement of mechanical properties for tablets to the compression stage.

I.2 Objectives

The objectives of the research were:

- To develop an empirical correlation for the mass transfer coefficient of pharmaceutical powders in a FBD.
- To study the behavior of the mass transfer coefficient ($k_g a$) before and after the critical moisture content (w_c) in the drying curve as a function of operating conditions.
- To study the effect of chemical properties of powders in the mass transfer process.

CHAPTER II: BACKGROUND AND LITERATURE REVIEW

II.1 Definition of fluidization

In many technological operations such as drying, it is often necessary to bring a granular material into intimate contact with a fluid (gas or liquid). In the simplest case, the fluid is forced to flow through a layer of particles, which rest one on top of the other and remain static relative to one another or to the walls of the vessel. Such a layer is termed as a *fixed bed* when a fluid flows through the particles. The fluid velocity in the spaces between the particles, known as the interstitial velocity, is greater than its velocity in the free cross section, which is known as the superficial velocity. At the state where the fluid velocity forces, the bed of particles to attain properties similar to those of fluids called incipient fluidizing velocity and the bed of particles is referred to a *fluidized bed*. The particles of a fluidized bed float in the fluid and intermix. Fluidization is said to be particulate if the volumetric concentration of solid particles is uniform throughout the bed and does not change with time (Vojtěch, (1966)).

II.2 Fluidized drying

Fluidized bed technology has been widely used in the pharmaceutical industry for drying, granulating, and coating. A fluid bed dryer significantly reduces drying time compared to a tray dryer or vacuum dryer, as indicated by Vojtěch (1966). It also exposes the entire product surface area to the high volume of air stream and heat is

transferred to the product surface by convection. However, if the inlet air velocity is not properly selected, consistent and uniform drying will not be obtained. Robinson (1992) described the importance of inlet air velocity in obtaining uniformity during fluid bed drying.

Fluid bed dryers (FBD) available for use in the pharmaceutical industry include two types, vertical and horizontal. Fluidized drying may be carried out as a batch or in a continuous process. In batch vertical FBDs, as the one used in this research, the fluidizing air stream is induced upward by a fan. The air is heated up to the required temperature and flows upward through the wet material, which is contained in a drying chamber fitted with a wire mesh support at the bottom. In continuous drying, the wet material enters the dryer as a continuous stream, and the dry material is also removed continuously maintaining the hold up in the dryer constant. Continuous horizontal dryers, suitable for pharmaceutical use, have a vibrating conveyor to move the granulation across the unit. This dryer can be divided in several zones with independent control of airflow and temperature. In addition, the rate of flow of the drying medium is usually such that the solids are thoroughly mixed, this being a characteristic feature of fluidized drying.

II.3 Drying curve

Drying is defined as a process of moisture removal due to simultaneous heat and mass transfers. Heat, necessary for evaporation, is supplied to the particles of the material and moisture vapors are removed from the material into the drying medium. Heat is transported by convection from the surroundings to the particle surface, and from there, by conduction, further into the particle. The moisture can be either transported to the surface of the product and then evaporated, or transported in the opposite direction

within the particle (as a liquid or vapor) to the surface and there it evaporates and passes by convection, to the surrounding. The heat transfer depends on the air temperature, relative humidity, airflow, exposed area and pressure.

Regardless of the type of dryer used, the solid particle is dried in a sequence of four steps as shown in Figure II.1. First, the particle is heated up to the required temperature, then the moisture from the wet surface is evaporated, after which the particle is partially dry. Finally, the particle surface is completely dried through a combination of internal evaporation and diffusion (Lipták, (1998)).

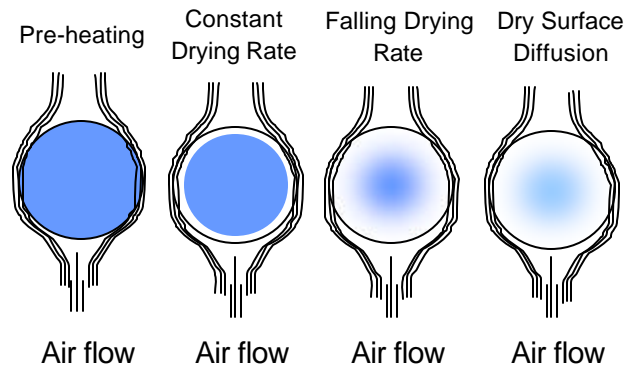


Figure II.1. Schematic diagram of the drying process in a particle

The simultaneous heat and mass transfer between the material being dried and the drying medium is typically characterized by a drying curve, which shows the dependence of the material MC with time. An example of typical forms of drying curves is shown in Figure II.2, where w_a is the initial MC, w_c is the critical MC and w_e is the final MC of the dried product. Figure II.2, section A-B represents the preheating stage of the product and the period where the operating conditions are reached. Since some heat is needed to bring the material to the initial drying temperature, evaporation during this phase is slow. In the next section B-C, surface moisture evaporates at a constant rate. The temperature

near the surface of the solid during this time is the wet bulb temperature of the air (Liptak, 1998) that is in direct contact with the product. The rate of evaporation drops off (section C-D) once the particle surface moisture has evaporated. This phenomenon is due, in part, to a case hardening of the surface, and in part to the long path necessary for the water to migrate from the bulk of the material to the surface. If the solid contains bound water, the rate will drop off even more as the bound moisture diffuses to the surface, represented by section D-E of the curve.

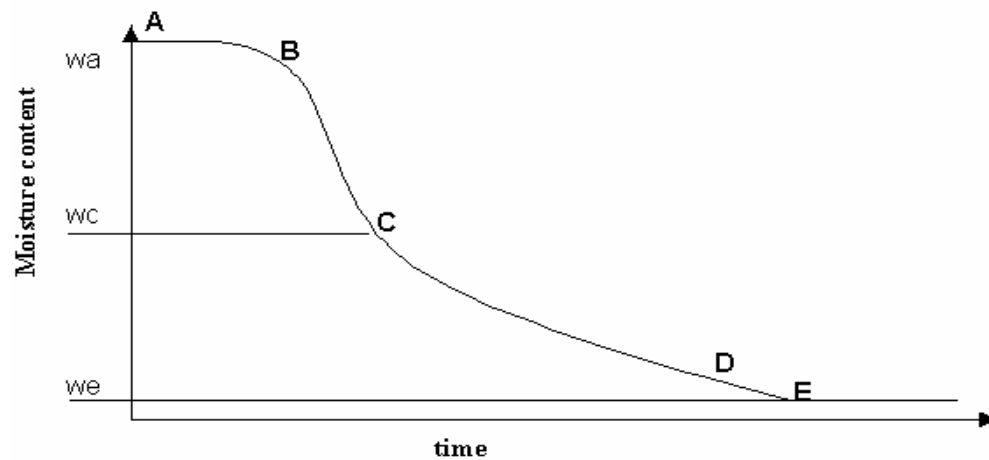


Figure II.2. Diagram of drying curves, where A-B is the preheating stage, B-C is the constant rate period, C-D is the falling rate period and D-E is the diffusion stage adopted by Lipták.

The derivative of the MC with respect to time is known as the rate of drying. The drying rate in each of the four phases of drying is depicted in Figure II.3. During the constant period (B-C), the rate of drying is controlled by external factors such as the rate of heat and mass transfer between the particle surface and the drying medium. In the falling rate period (C-D), the conduction of heat and diffusion of moisture within the particle is the rate controlling phenomena. The rate of drying depends in this region on

the internal drying factors, which practically cannot be influenced by fluidization. The critical moisture content appears between the constant and falling rate period, which represent superficial area when the particle is dried. Drying time is mostly the two stages, *constant and falling rates*.

The rate of drying of wet solid is a function of the difference in MC (driving force) between the material and the drying fluid, surface area, and mass transfer coefficient $k_g a$. For mass transfer at temperatures well below the boiling point of the moisture, the driving force for the transport between the surface of the material and the drying medium is given by the difference in partial pressure, or concentrations.

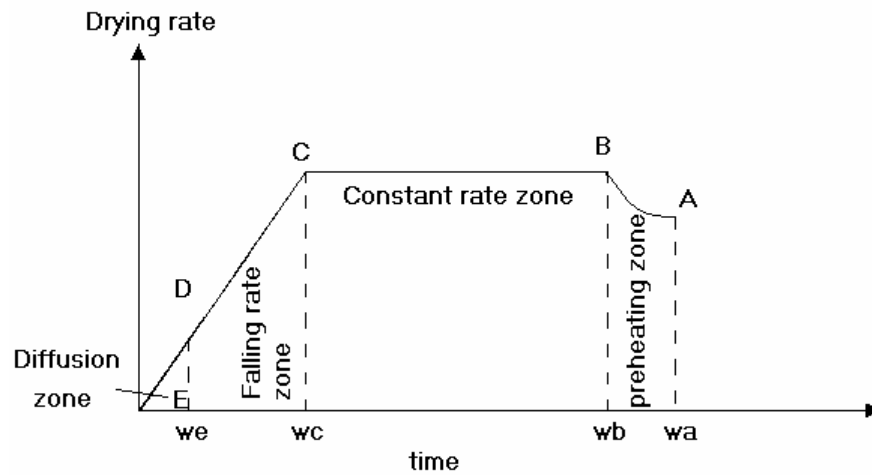


Figure II.3. Diagram of drying rate zones

The rate at which moisture evaporates from the surface can be described in terms of a gas mass-transfer coefficient k_y and the difference in humidity of the gas at the liquid gas interface (Y_s) and the bulk of the stream (Y). N_c is the constant water flux described by

$$N_c = k_y (Y_s - Y) \quad [\text{II.1}]$$

In batch drying, the coefficient k_y may be expected to be constant for each drying stage but not for the entire process. One reason for this is that when the MC has reached a critical point, the surface film of moisture has been reduced considerably by evaporation. Further drying causes dry spots to appear upon the surface. At this point, diffusion dominates the process.

II.4 Drying models

Many studies have been conducted to model fluid bed processes using transport phenomena principles for mass, momentum, and heat transfer (Mikami (1998), Hjertager (1999), Wang and Chen (1999, 2000) and even using more sophisticated modeling (Seibert and Burns (1996)). However, their mathematical complexity, computational load, and inability to prove precise predictions on a completely theoretical basis of experimental results make these alternatives still inappropriate for industrial implementation.

Bennett (1982) mentioned that during the constant rate period, water is supplied from the solid near the surface fast enough to keep the surface entirely wet. Applying a water balance (w) in the solids

$$\frac{dw}{dt} = RA \quad [\text{II.2}]$$

$$w = m_s X \quad [\text{II.3}]$$

$$m_s \frac{dX}{dt} = RA \quad [\text{II.4}]$$

Integrating Eq. II.4, Eq. II.5 can be obtained to calculate MCs for batch drying operations.

$$t = \frac{m_s}{AR}(X_0 - X_1) \quad [\text{II.5}]$$

where t is the drying time, m_s is the weight of dry solid, R is the drying rate, A is the wet surface area and X is the moisture contents.

Shinskey (1979) presented Eq. II.13 to predict the drying rate for the constant rate period. This equation comes from a combination of an energy and a mass balance. Eq. II.6 presents an energy balance between the heat given away by the drying medium and the energy required by the water evaporated.

$$T_g - T_w = \frac{I_w(Y'_w - Y_w)}{h_g / k_y} \quad [\text{II.6}]$$

where T_g is the temperature of gas, T_w is the wet bulb temperature, λ_w is the latent heat of water, Y'_w is the humidity at the interface, Y_w is the humidity in the medium, h_g is the heat transfer coefficient and k_y is a mass transfer coefficient.

Using the definitions for the molar flux (N_A) (Treybal, 1982)

$$N_A = k_a(\bar{P}_{Ag} - P_{Aw}) \text{ or } N_A = k_y(Y'_w - Y_w) \quad [\text{II.7}]$$

where \bar{P}_{Ag} is the vapor pressure in the surface and P_{Aw} is the partial pressure in the medium.

A mass balance of water (w) is presented in Eq. II.8 that together with Eq. II.7 produce Eq. II.9.

$$dw = N_A dA \quad [\text{II.8}]$$

$$\frac{dw}{dA} = k_y(Y'_w - Y_w) \quad [\text{II.9}]$$

Defining a mass transfer coefficient $z = \frac{h_g}{I_w}$ (Shinskey, (1979)) and using log mean

temperature (**LMTD**), and rearranging the equations presented before, Eq. II.13 is

obtained integrating Eq. II.12 from 0 to a , and from inlet Temperature (T_i) and outlet Temperature (T_o), the Shinskey's model is obtained

$$\frac{h_g}{I_w}(t_g - t_w) = k_y(Y'_w - Y_w) \quad [\text{II.10}]$$

$$dA \frac{h_g}{I_w}(t_g - t_w) = dw \quad [\text{II.11}]$$

$$dA z \ln \frac{(T_o - T_w)}{(T_i - T_w)} = dw \quad [\text{II.12}]$$

$$(w_2 - w_1) = a * z \ln \frac{(T_o - T_w)}{(T_i - T_w)} \quad [\text{II.13}]$$

where Δw is the drying rate, a is the solid surface area, T_i is the air inlet temperature, T_o is the air outlet temperature, T_w is the air wet bulb temperature, and z is the mass transfer coefficient equal to $\frac{950 * k_g}{I_w}$ for water-air system. k_g is the studied mass transfer coefficients and I_w is the latent heat of water.

The falling rate period begins as soon as the interface temperature starts to increase and the driving force for drying starts to decrease. During this period, an increase of the mass transfer resistance leads to reduce the interface moisture content as well as lower interface air humidity. The effect of a higher value of $k_g a$ is thus partially compensated by a decrease in the driving force. An internal diffusion resistance in the drying material is the primary control of the speed of the drying process.

Lipták *et al.* (1998) presented the Shinskey's model, Eq. II.18, for the falling rate period. In this region, the rate of drying is proportional to the ratio of the actual to the critical moisture content ($\frac{w_p}{w_c}$). Modifying Eq. II.12 with the ratio of moisture and the definition of ζ , Eq. II.14 is obtained.

$$dA \left(\frac{k_g a 950}{I_w} \right) \left(\frac{w_p}{w_c} \right) \ln \frac{(T_o - T_w)}{(T_i - T_w)} = dw \quad [\text{II.14}]$$

Evaporation of moisture into a flow F_a of air results in a decrease in dry-bulb temperature proportional to the ratio of the heat capacity C_p of the air and the latent heat I_w of the water.

$$- F_a C_p \frac{dT}{I_w} = dw \quad [\text{II.15}]$$

Substituting and integrating from inlet (i) to outlet (o) gives a solution relating temperature and the total surface area needed for the mass transfer.

$$\int_0^a dA = \frac{F_a C_p}{950 k_g \frac{w_p}{w_c}} \int_{T_i}^{T_o} \frac{-dT}{T - T_w} \quad [\text{II.16}]$$

$$a = \frac{F_a C_p}{950 k_g \frac{w_p}{w_c}} \ln \left(\frac{T_i - T_w}{T_o - T_w} \right) \quad [\text{II.17}]$$

Then, the solid's moisture can be obtained as a function of the inlet, outlet, and wet bulb temperatures by rearranging Eq. II.17.

$$w_p = \frac{w_c F_a C_p}{950 k_g a} \ln \left(\frac{T_i - T_w}{T_o - T_w} \right) \quad [\text{II.18}]$$

where w_p is the product moisture content, w_c is the critical moisture content, a is the solid surface area, C_p is the specific heat of air, F_a is the air flow, T_i is the air inlet temperature, T_o is the air outlet temperature, T_w is the air wet bulb temperature, and k_g is the mass transfer coefficient.

There also exist completely empirical models to predict the MC of powders. Robinson (1992) presents a Temperature Drop model (TD). The TD for batch drying process is given by

$$w_p = A (\Delta T)^b - C (\Delta t)^d \quad [\text{II.19}]$$

where w_p is the product MC, ΔT is the temperature drop of the drying gas across the product, Δt is the drying time and A , C , b , d are the empirical parameters. This actually is one of the most common models used to control product MC due to the little process information required and uniform process conditions used between batches in the industry.

The temperature drop method enables calculation of drying rates and rate of change in drying rates for use as the controlled variables. Such variables significantly improve dryer control of endpoint MC because they are independent of dryer and process variable. Therefore, Robinson mentioned that it is easy to determine the MC at any point along the dryer using resistance temperature detectors and thermocouples.

Another empirical correlation to determine the final MC is the Temperature Difference (ΔT) technique, Alden *et. al.* (1988). This method only considers inlet, outlet, saturated wet material temperatures, and also uses parameters such as MC of the incoming drying air. The ΔT technique proved to control product MC in a narrower range. The technique also proved to be unaffected by the relative humidity changes of the drying air.

The empirical models were found to determine the endpoint MC but only consider parameters such as Temperature due to control process; a minimum of parameters are needed to count.

II.5 Mass transfer in Fluid Bed Dryers

II.5.1 Mass transfer coefficients

The definition of the mass transfer is based on empirical observations like the ones those used in developing Fick's law. The amount of mass transferred is proportional to the concentration difference and the interfacial area. An experimental factor k , called mass transfer coefficients is added to establish the equality. From the mechanism of mass transfer, it can be expected that the coefficient k would depend on diffusivity D_v , and on the variables that control the dynamics of the fluid flow, namely, the velocity u , the viscosity μ , the density ρ , and some linear dimension D .

$$k = f(D_v, D, u, \mathbf{m}, \mathbf{r}) \quad [\text{II.20}]$$

Dimensionless analysis gives

$$\frac{kD}{D_v} = f\left(\frac{Du\mathbf{r}}{\mathbf{m}}, \frac{\mathbf{m}}{rD_v}\right) \quad [\text{II.21}]$$

Studies of mass transfer in packed bed are presented by McCabe *et. al.* (1993). They presented equations of mass transfer from liquids or gases to particles in packed beds. They found that the coefficients varied with the square root of the mass velocity and two-thirds power of the diffusivity. Eq. II.22 is recommended for spheres or roughly spherical solid particles that form a bed with about 40 to 45 percent voids. For cylindrical particles these equations can be used with the diameter of the cylinder in Re and Sh .

$$Sh = 1.17 Re^{0.585} Sc^{1/3} \quad [II.22]$$

where Sh is the Sherwood number, Re is the Reynolds number (Eq. II.23) and Sc is the Schmidt number (Eq. II.24)

$$Re = \frac{d_p G'}{m} \quad [II.23]$$

$$Sc = \frac{m}{D r} \quad [II.24]$$

Treybal (1978) provided several equations for the mass transfer coefficients. For example, Eq. II.25 applies for a fluid through fixed beds of pellets

$$J_D = \frac{20.4}{\epsilon} Re^{-0.815} \quad [II.25]$$

where ϵ is the porosity of the powders, J_D is the mass transfer dimensionless group ($StSc^{2/3}$), Re is the Reynolds number, and Sc is the Schmidt number.

Siettos (1999) presented a correlation for the mass transfer coefficient in a FBD. He also presented a mathematical model involving, chiefly, heat and mass transfer balances within the drying drum for the gas and solid phase. It was assumed that a multi-dispersed solid with known mass distribution of particles of uniform material moisture content and temperature enters the dryer where complete mixing prevails for the phases involved. The mass transfer coefficient (K_M) was modeled using first order kinetics. For fluid bed dryers, he proposed that the mass transfer coefficients follow

$$K_M = k_0 d_p^{k_1} T_A^{k_2} V_G^{k_3} X_s^{k_4} \quad [II.26]$$

where d_p is the average particle diameter, T_a is the air temperature at the dryer exit, V_g is the air velocity, X_s is the material moisture content at the dryer exit and k_{0-4} are adjusting parameters.

Chen et al. (1999) performed a study for the mass transfer coefficient using a centrifugal fluid bed dryer. It was assumed that the heat loss was negligible, the particles were dispersed in the air stream and that the physical properties of granules and air were stable during the drying process. He found that the mass transfer coefficients were affected by factors such as particle size (d_p), air density (ρ), air viscosity (μ) and the diffusivity (D_{AB}). The following correlation was proposed:

$$Sh = k_0 Re^{k_1} F_c^{k_2} N_b^{k_3} \quad [\text{II.27}]$$

where Sh is the Sherwood number, Re is the Reynolds number, the F_c is the centrifugal factor and N_b is the ratio of h/d_p where d_p is the particle diameter and h is the bed thickness, and k_0 to k_3 are adjusting parameters. The adjusting parameters results were $k_0=0.00015$, $k_1=1.99$, $k_2=-0.13$ and $k_3=0.05$.

Bennett (1982) presented an equation for the mass transfer coefficients for solid spheres, which is the standard shape for analyzing pharmaceutical powders. Other investigators have also employed spheres of solid material, which have either sublimed into passing air streams or dissolved into a passing stream of liquid. The mass transfer coefficient equation for these cases is

$$\frac{k_p D}{D_{AB}} = 2 + 0.6 \left(\frac{\mu}{\rho D_{AB}} \right)^{1/3} \left(\frac{D u_o \rho}{\mu} \right)^{1/2} \quad [\text{II.28}]$$

where D_{AB} is the diffusivity of A, μ is the viscosity of air, ρ is the air density, u_o is the superficial velocity and k_p is the mass transfer coefficient. The constant two (2) is based

on a system in which molecular diffusion of a single component occurs at a steady state outward from a spherical surface into an infinite, stagnant medium. The second term on the right-hand side of Eq. II.28 represents the contribution of the fluid motion to mass transfer from the sphere.

Oldshue (1989) mentioned a method involving the particle Sherwood number ($k_L d_p / D$) as a function of particle Reynolds number ($u d_p / \nu$), where u is the average relative velocity between fluid and solid. The relative velocity is a function of power input and fluid viscosity. He also presented a correlation (II.29) of the mass transfer coefficients involving the dependency with the particle Reynolds number. The equation is

$$\frac{k_L d_p}{D} Sc^{1/3} = f\left(\frac{P/V(d_p)^4}{u}\right)^{1/3} \quad [\text{II.29}]$$

P is the concentration of product, V is the reactor volume, k_L is the mass transfer coefficient, D is the impeller diameter, Sc is the Schmidt number, d_p is the mean particle diameter, and u is the average relative velocity between fluid and solid. Another method that Oldshue presented is based on the slip velocity and the terminal velocity of the particle. The equation is

$$k_g J_s = E k_{gt} \quad [\text{II.30}]$$

where E is an enhancement factor, which depends only on the particle diameter, k_g is the mass transfer coefficient, k_{gt} is the mass transfer coefficient for solids in a free fall and J_s is the mass flux.

Mass transfer is a complex process governed by factors such as airflow velocity, particle size, porosity, temperatures and other parameters. Even now, in design and

optimization of drying processes, there is a great need for stable and reliable models to quantify or predict drying rates and drying time with satisfactory accuracy.

Therefore, it would be significant to contribute to the understanding of the behavior of the mass transfer coefficients ($k_g a$) along the entire drying process of pharmaceutical powders.

CHAPTER III: MATERIALS AND METHODS

III.1 Materials for drying curve experiments

The materials used in the preparation of the pharmaceutical granulation that has to be dried are included in Table III.1. Three different granulations were prepared to develop the experiments. Formulation 1 was used to develop the empirical correlations and formulations 2 and 3 were used for varying composition experiments.

Table III.1. List of ingredients for pharmaceutical granulation

Ingredients	Specification	w/w%
Lactose Monohydrate*	<i>Formulation 1</i> Ph. Eur/USP-NF/ JP GranuLac 70 Function: Diluent	80%
	<i>Formulation 2</i> USP-NF XXIII Forestmost © product 315 Spray dried, 140 Mesh Function: Diluent	
Lactose Anhydrous	<i>Formulation 3</i> USP-NF Direct tableting Function: Diluent	80%
Pregelatinized Starch	USP-NF XXIII Colorcon © product 1500 Functions: Diluent, Binder and Desintegrant	13%
Distilled Water	Distilled / pH: 5.50-6.50 Conductivity: 1.8 $\mu\text{S}/\text{cm} \pm (24^{\circ}\text{C})$	7%

*Lactose monohydrate was the altered ingredient in the formulation.

III.1.2 Equipment for drying curves experiments

Ingredients were weighed and mixed in a Littleford High Shear Mixer with a capacity of 20 kg. The mixer consists of a cylindrical chamber, upper and lower sealed doors, a main shaft with four paddles (two with a shape of V and two near the sidewalls to prevent dead volume), and two motors.

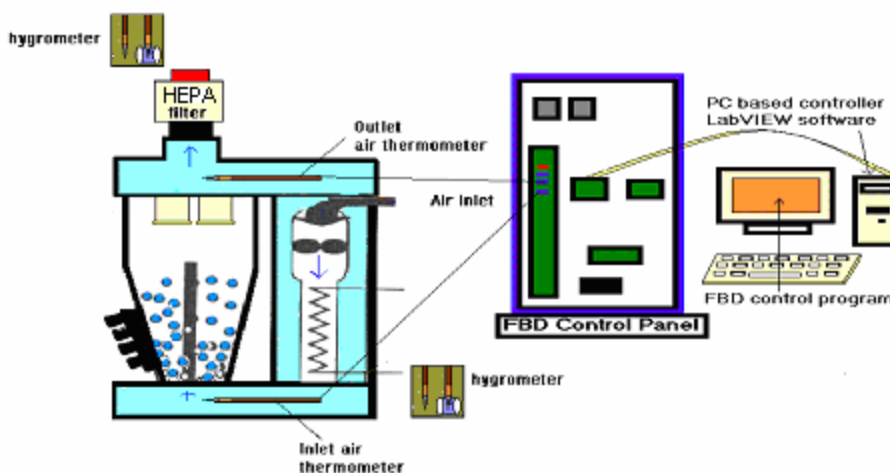


Figure III.1. Schematic of Fluid Bed Dryer and control panel

Figure III.1 shows a schematic of diagram FBD and the control panel used for drying experiments. The formulations were dried in a Fluid Bed Dryer (FBD) Aeromatic AG STREA 1 model. It consists of a blower with operating conditions between 0-120 m³/hr of airflow, an electrical resistance, and a conical recipient bowl with a product container of 16.5 L. The operating temperatures of inlet dry air were in the range of 50 to 100°C. Accessories used were a 200 wire mesh product bottom screen, a plate to enhance the fluidization of fine granulations with a 22% free cross sectional air

distribution, a bypass tube, and nylon T695 exhaust air filters. A HEPA filter was placed at the air exit of the equipment.

The samples were analyzed with a Metler Toledo LJ 16 Infrared Moisture Analyzer with a standard balance. The temperature can be programmed from 50 to 160°C. The drying times can be set between 10 to 15 minutes. The drying process can be controlled automatically and the result is displayed in grams or in terms of mass percent of water removed.

Additional accessories used to conduct the drying curve experiments include Taylor hygrometers to measure dry and wet bulb temperature of the inlet and outlet air, and thermocouples. These were installed at the entrance and exit of air to the product recipient. Thermocouples were type J transition probe ungrounded type Teflon® insulated wires. Temperature ranges for the probes: -100 to 300°C.

III 1.3 Methodology for drying curves experiments

This section is divided by the unit operation used in the experiments and the description is presented in the order used.

III 1.3.1 Powder weighing

Recipients or containers were thoroughly cleaned and dried before adding the bulk materials. Ingredients for pharmaceutical formulation were weighed. Table III.1 describes the ingredients used with the specifications and the quantities for the batch size. The ingredients were placed in the Littlerford High Shear Mixer/Granulator after weighing.

III 1.3.2 Wet granulation preparation

Before adding the powders to starting the mixing operations, the mixer was thoroughly cleaned and entirely dried prior. Approximately half of the ingredients were added in such a way as to cover the mixer's entire bottom. The remaining ingredients were distributed as evenly as possible on top of the previously added layer. The remaining half of the ingredients was added. This is called sandwich addition of the ingredients. Dry mixing was performed for 5 minutes. The mixer was turned off to take a sample for the determination of MC. Then, the mixer was turned on and the distilled water was added in the provided recipients. The mixing process time continued for 45 minutes. Representative samples of the granulation were taken for analysis of the MC with the Moisture Analyzer.

III 1.3.3 Fluid bed drying

Prior to starting drying, the dryer bowl was thoroughly cleaned and dried. The empty dryer bowl was preheated or conditioned until it reached the operational conditions. The wet granulation was divided in containers of 1 kg each and added to the dryer bowl once at a time. The required devices, inlet and outlet hygrometer were located at the bottom and top of the fluid bed dryer. The operating conditions were typed into the Fluid Bed Dryer Control Program. Product samples were withdrawn every three minutes. These intervals could change depending on the operating conditions. The airflow velocity and drying temperature were set up at the start of the drying process depending on the experiment. Data of inlet and outlet, wet and dry bulb temperatures were collected during the drying process. When the drying process was finished, the containers were allowed to cool for 10 to 15 minutes.

Table III.2 presents the operating conditions used in the Fluid Bed Dryers. The mass load was 1 kg, the drying temperatures were 60 and 80°C and the air flow (AF) were between 40 to 80 m³/hr. An experimental design was proposed to develop the experiments.

Table III.2. Operating conditions used at the FBD

Air velocity (m ³ /hr)	Mass load (kg)	Drying temperature (°C)	Initial MC (%w/w)
40	1.0	60, 80	~9.0
50	1.0 kg	60, 80	~9.0
60	1.0 kg	60, 80	~9.0
70	1.0 kg	60, 80	~9.0
80	1.0 kg	60, 80	~9.0

III 1.3.4 LOD moisture analyzer

The balance, the printer and the heater were turned on. All aluminum-weighing trays were completely cleaned and dried prior to using. To start with the LOD analysis, the aluminum plate was tared. Between 5.000 and 5.500 g of the samples were weighed. The samples were distributed uniformly in the tray. Temperature was set to 130 °C and the drying time to 15 minutes. Before starting the next analysis, the instrument was allowed to cool down.

CHAPTER IV. SAMPLE CALCULATION

This chapter includes a sample calculation for the mass transfer coefficient correlation. This correlation will be used to predict the MC in the granulation. All experimental runs were performed in triplicates to determine the reproducibility of results. The third replicate in each run was used to validate the empirical correlation.

IV.1 Drying curve

The average moisture content was calculated for all experiments to generate the drying curves. The averages MC were calculated using Eq. IV.1.

$$\overline{MC} = \frac{(MC_1 + MC_2)}{2} \quad [IV.1]$$

where MC_1 and MC_2 are the MC in replicate 1 and 2 respectively. Table IV.1 includes the actual data for the operating conditions of $AF=60 \text{ m}^3/\text{hr}$ and $T=60 \text{ }^\circ\text{C}$, and the results of \overline{MC} . Example of \overline{MC} calculation for a drying time of 3 min is:

$$\overline{MC} = \frac{(7.6\% + 8.5\%)}{2} = 8.05\%$$

To develop a statistical analysis in the obtained results, the residual's percent MC standard deviation (σ) was calculated using Eq. IV.2.

$$s = \left(\frac{\sum_{i=1}^2 (\%MC_i - \overline{MC})^2}{\text{number of test} - 1} \right)^{\frac{1}{2}} \quad [IV.2]$$

$$s = \left(\frac{(7.6 - 8.05)^2 + (8.5 - 8.05)^2}{2 - 1} \right)^{\frac{1}{2}} = 0.636$$

Eq. IV.3 was used to calculate the 95 % confidence interval

$$95 \% \text{ confidence interval} = \left(AveMC \pm \frac{t_{\alpha/2} * (\text{standard deviation})}{(\text{number of test})^{0.5}} \right) \quad [IV.3]$$

$$95 \% \text{ confidence interval} = \left(8.05 + \frac{12.706 * (0.636)}{(2)^{0.5}} \right) = 13.76$$

$$95 \% \text{ confidence interval} = \left(8.05 - \frac{12.706 * (0.636)}{(2)^{0.5}} \right) = 2.33$$

where the value of $t_{\alpha/2}=12.706$ is suggested by Montgomery (1996). Similar calculations

were performed for all collected data.

Table IV.1. Experimental results of MC and statistical analysis for AF=60 m³/hr and T=60 °C

Time/min	MC ₁ (%)	MC ₂ (%)	\overline{MC} (%)	Std dev	95% CI
0	9.81	9.3	9.56	0.360	(11.29,4.80)
3	7.6	8.5	8.05	0.636	(13.76,2.33)
6	6.29	6.9	6.60	0.431	(11.92,4.17)
9	5.89	6.5	6.20	0.431	(11.62,4.17)
12	5.61	5.61	5.61	0.000	(5.61,5.61)
15	5.49	5.7	5.60	0.148	(6.15,4.82)
18	5.1	5.6	5.35	0.354	(6.69,3.51)
21	5.31	5.5	5.41	0.134	(5.91,4.70)
24	5.29	5.21	5.25	0.0566	(5.54,5.04)
27	5.3	5.19	5.25	0.0778	(5.65,4.95)
30	5.3	5	5.15	0.212	(6.23,4.34)

Once the \overline{MC} is calculated, drying curves were plotted as shown in Fig. IV.1 for $AF=60 \text{ m}^3/\text{hr}$ and $T=60 \text{ }^\circ\text{C}$. The average drying curve was then used to establish the critical MC.

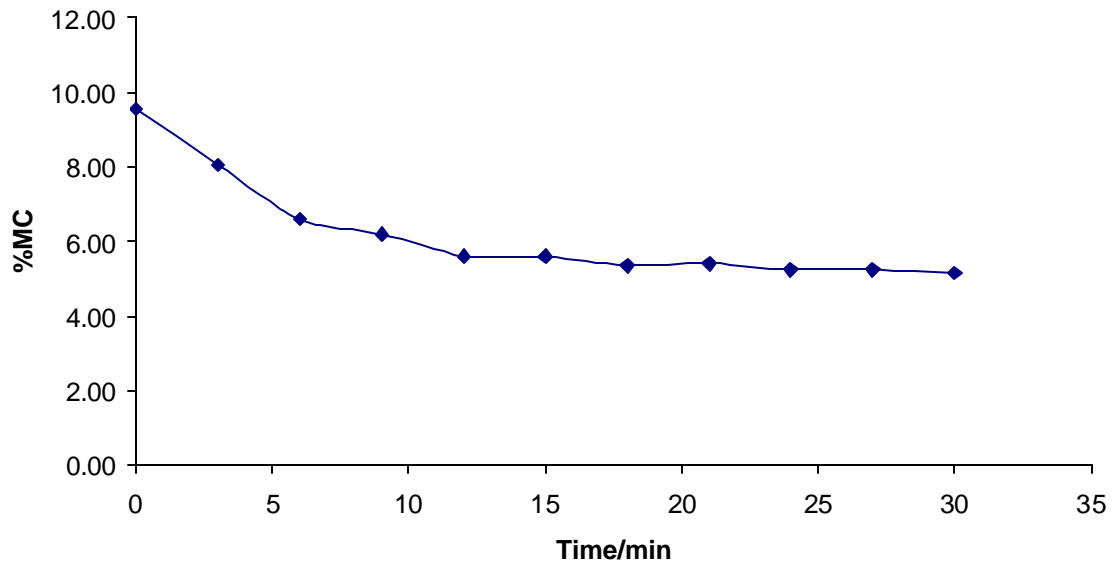


Figure IV.1. Drying curve for operating conditions of $AF=60 \text{ m}^3/\text{hr}$ and $T=60 \text{ }^\circ\text{C}$

IV.2 Mass transfer coefficients

To determine the empirical correlation for the mass transfer coefficient (k_{ga}), the drying curve was divided first, in two regions, the constant drying and the falling rates, based on the critical MC (w_c).

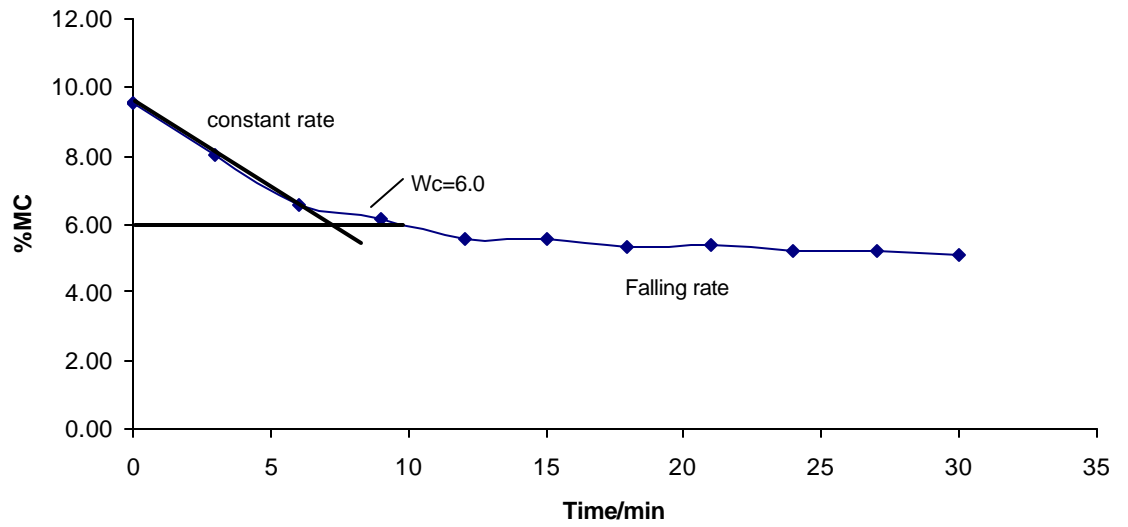


Figure IV.2. Graphical procedure to determine the critical MC

Figure IV.2 depicts the procedure to obtain w_c for all the runs. The result for Figure IV.1 was approximately 6.0 % of MC, similar results were obtained for all runs. Table IV.2 includes additional average data for the operating conditions of $AF=60 \text{ m}^3/\text{hr}$ and $T=60^\circ\text{C}$.

Table IV.2. Average data of temperature for the operating conditions of $AF=60 \text{ m}^3/\text{hr}$ and $T=60^\circ\text{C}$

Time (min)	$T_{\text{out}} (^\circ\text{C})$	$T_{\text{in}} (^\circ\text{C})$	$T_w \text{ in (F)}$	$T_w \text{ out (F)}$
0	25.98	60.96	61.00	68.50
3	28.52	60.25	60.50	69.50
6	30.57	60.94	62.90	69.00
9	33.11	62.40	63.00	67.75
12	35.64	61.72	61.50	69.00
15	37.99	60.94	63.05	69.50
18	39.75	61.72	63.00	71.00
21	41.60	62.11	63.50	71.25
24	42.68	61.92	62.50	71.50
27	43.85	61.13	63.50	71.50
30	44.73	61.23	63.50	72.00

IV.2.1 Constant rate region

For the evaluation of the constant rate period, data was evaluated from the beginning of the experiment up to the critical moisture. Eq. II.13 was rearranged to obtain $k_g a$.

$$k_g a = \frac{(w_2 - w_1) * I_w}{950} * \ln \left(\frac{T_o - T_w}{T_i - T_w} \right)$$

Steam tables (Smith and Van Ness, 1987) were used to estimate the latent heat of water (λ_w) for the average temperature (T_{ave}) of the air inside the dryer. An equation to predict λ_w for water is obtained

$$I_w = (A * T_{ave}) + B \quad [IV.4]$$

$$I_w = (-43.478 \frac{J}{molK^2} * T_{ave}(K)) + 56938 \frac{J}{molK}$$

where T_{ave} is the average temperature as calculated by Eq. IV.5; for water $A=-43.478$ and $B=56938$. Using data from Table IV.2, the average temperature in the dryer at $t=3$ minutes was

$$T_{ave} = \frac{(T_{in} + T_{out})}{2} \quad [IV.5]$$

$$T_{ave} = \frac{(60.25^\circ C + 28.52^\circ C)}{2} = 44.38^\circ C = 317.53 K$$

$$I_w = (-43.478 \frac{J}{molK^2} * 317.53K) + 56938 \frac{J}{molK} = 43132.43 J/mol_{water}K$$

The amount of granulation inside the dryer at 3 minutes of drying has to be considered in the calculation of the evaporation rate (Dw). For example, the batch initially had 1000 grams with a 10 grams sample withdrawn every 3 minutes. Therefore, the dryer

bowl has 980 grams of the granulation at 3 minutes of drying. Eq. IV.6 through IV.8 were used to calculate the ΔW at 3 minutes for AF=60 m³/hr and T=60 °C, where the value obtained for W₂ was 63.97 in grams of water.

$$W = \frac{\%MC}{100} * \text{total mass in dryer} \quad [IV.6]$$

$$W_1 = \frac{8.05\%}{100} * 980g = 78.89 \text{ g}_{\text{water}}$$

$$\Delta W = W_2 - W_1 = 63.97g - 78.89g = -14.92 \text{ g}_{\text{water}} \quad [IV.7]$$

$$\Delta w = \frac{\Delta W}{\Delta t} = \frac{-14.92g}{3 \text{ min}} = -4.97 \text{ g}_{\text{water}} / \text{min} \quad [IV.8]$$

$$\text{or } \Delta w = 0.00459 \text{ mol/s}$$

\bar{T}_w was calculated as $\bar{T}_w = \frac{T_{\text{wet in}} + T_{\text{wet out}}}{2} = 18.33^\circ C$. Substituting these results in $k_g a$,

it is obtained,

$$k_g a = \frac{-0.00459 \frac{\text{mol}}{\text{s}} * 43132.43 \frac{\text{J}}{\text{molK}}}{950 \frac{\text{J}}{\text{kgK}}} \ln \left(\frac{28.50^\circ C - 18.33^\circ C}{62.40^\circ C - 18.33^\circ C} \right) = 0.147 \text{ kg/s}$$

The results of $k_g a$ for constant rate period are included in Table IV.3.

Table IV.3. Results of $k_g a$ for the constant rate period for operating conditions of AF=60 m³/hr and T=60 °C

Time (min)	$k_g a$ (kg/s)
0	0.129
3	0.147
6	0.138
9	0.0492

IV.2.2 Falling rate region

Eq. II.18 was used to calculate the experimental values of $k_g a$ for the falling rate period. Data from Table IV.1 and IV.2 were used to calculate the experimental $k_g a$. Rearranging the equation for $k_g a$ gives:

$$k_g a = \frac{w_c F_a C_p}{w_p 950} \ln \frac{(T_{in} - T_w)}{(T_{out} - T_w)}$$

The specific heat (C_p) values of air were estimated with standard data and Eq. IV.9.

$$C_p = C_{pair,ig} = R(A + BT + CT^2 + DT^{-2}) \quad [IV.9]$$

The values for the constant in Eq. IV.9 are $A = 3.355$, $B = 0.575 \times 10^{-3}$, $C = 0$, $D = -1.60 \times 10^3$, (Smith and Van Ness, 1987) and $R = 8.314$ J/mol·K. For this case the result of C_p for 12 minutes:

$$T_{ave} = \frac{(T_{in} + T_{out})}{2} = \frac{61.72 + 35.64}{2} = 48.68^\circ C = 321.83K$$

$$C_p = 8.314 \frac{J}{molK} (3.355K + 0.575 * 10^{-3} (321.83K) + C(321.83K)^2 + D(321.83K)^{-2}) = 29.31 \frac{J}{mol_{air}}$$

The molar flow rate (F_a) was calculated using the ideal gases law, Eq. IV.10.

$$F_a = \frac{P * v}{R T_{in}} \quad [IV.10]$$

where P is the pressure, v is the air volumetric flow rate. The temperature used in this calculation corresponds to the total average inlet temperature calculated as per Eq. IV.11.

$$\overline{T_{in}} = \frac{\sum T_{in} runs}{\text{number of run}} \quad [IV.11]$$

$$\overline{T_{in}} = \frac{(60.96 + 60.25 + 60.94 + 62.40 + 61.72 + 60.94 + 61.72 + 62.11 + 61.92 + 61.13 + 61.23) ^\circ C}{11}$$

$$\overline{T_{in}} = 61.39 ^\circ C = 334.54 K$$

The volumetric air flow at this condition was 60 m³/hr.

$$F_a = \frac{101325 \frac{N}{m^2} * (60 \frac{m^3}{hr}) * 1hr / 3600 s}{8.314 \frac{J}{molK} * 334.54 K} = 0.60716 \frac{mol}{s}$$

Substituting previous results, $k_g a$ for the falling rate period can be calculated as follow

$$k_g a = \frac{6\% * 0.60716 \frac{mol}{s} * 29.31 \frac{J}{molK}}{5.61\% * 950 \frac{J}{molK}} \ln \left(\frac{61.72 K - 18.47 K}{35.64 K - 18.47 K} \right) = 0.01851 \frac{kg}{s}$$

The summarized results of $k_g a$ for falling rate are shown in Table IV.4.

Table IV.4. Results of $k_g a$ for falling rate period with operating conditions of AF=60 m³/hr, and T=60 °C

Time (min)	$k_g a$ (kg/s)
12	0.01851
15	0.01594
18	0.01542
21	0.01373
24	0.01292
27	0.01159
30	0.01112

IV.3 Development of the empirical correlation

The empirical correlation shown in Eq. IV.12 was used to fit the experimental values of the $k_g a$

$$Sh = a Sc^b Re^c \quad [IV.12]$$

where Sh is the Sherwood number, Sc is the Schmidt, Re is the Reynolds number, and a , b , and c are the adjusting parameters. Substituting the previous data obtained in section IV.2 into Eq. IV.12, the values of Sh , Re and Sc were calculated.

To calculate Sh and Sc , the diffusivity (D_{AB} in cm^2/s) must be computed first using Eq. IV.13 (from Bird *et al.* (2002)).

$$D_{AB} = 0.0018583 \sqrt{T^3 \left(\frac{1}{M_A} + \frac{1}{M_B} \right)} * \left(\frac{1}{r s_{AB}^2 \Omega_{D_{AB}}} \right) \quad [IV.13]$$

where A is water and B is air, M_A is the molar mass for A = 18.015 g/mol and M_B is the molar mass for B = 29 g/mol and s_{AB}^2 is the collision coefficient $t = \frac{1}{2}(s_A + s_B) = 3.129$ and e_{AB} is the maximum attractive energy between two molecules = $\sqrt{e_A e_B} = 280.15 \text{ K}$ and $\Omega_{D_{AB}}$ is the collision integral

$$\Omega_{D_{AB}} = \frac{1.06036}{T^{*0.15610}} + \frac{0.19300}{\exp(0.47635T^*)} + \frac{1.03587}{\exp(1.52996T^*)} + \frac{1.76474}{\exp(3.89411T^*)} = 1.35$$

where, $T^* = \frac{k\bar{T}}{e_{AB}} = 1.45$ and $\frac{e_{AB}}{k} = 320.90$ and $\bar{T} = 320.90 \text{ K}$. Therefore, the results of

D_{AB} was $0.2425 \text{ cm}^2/\text{s}$.

For the calculation of Sh the diameter used was the diameter of the entrance of air to the FBD bowl as shown in Figure IV.3.

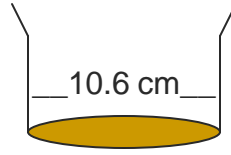


Figure IV.3. Diagram of the FBD bottom to establish the diameter for $k_g a$ correlations

The values of $k_g a$ obtained (in kg/s) had to be changed to cm/s to have unit consistency. For a specific value of 0.02 kg/s, the corresponding value is

$$\frac{k_g a \left[\frac{kg}{s} \right]}{r_w \left[\frac{g}{cm^3} \right] * a \left[cm^2 \right] * \frac{1}{1000} \left[\frac{kg}{g} \right]} = 0.227 \text{ cm/s}$$

The density of water (ρ_w) was obtained using a linear regression in the temperature range of 50-90°C, where the equation outcome was

$$\rho_w = -0.0006 \text{ g/cm}^3 \text{K} * \bar{T} (\text{K}) + 1.1905 \text{ g/cm}^3$$

$$\rho_w = -0.0006 \text{ g/cm}^3 \text{K} * (320.90 \text{K}) + 1.1905 \text{ g/cm}^3 = 0.998 \text{ g/cm}^3.$$

Figure IV.4 depicts the data used to determine the correlation to compute ρ_{water} .

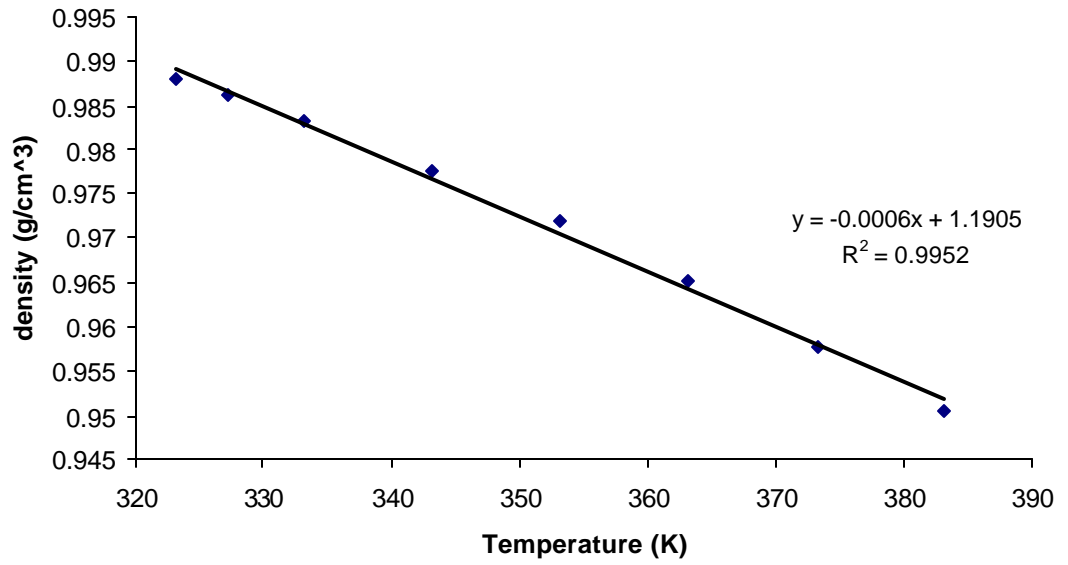


Figure IV.4. Experimental values of density of water vs temperature

Substituting the previous results, it is obtained,

$$Sh = \frac{0.2272 \frac{cm}{s} * 10.6cm}{0.2425 \frac{cm^2}{s}} = 9.93$$

To calculate the Re , the viscosity (m in g/ms) was determined using Eq. IV.14 (Bird *et al.* (2002)).

$$m = 0.0000266 \frac{\sqrt{MT}}{s^2 \Omega_m} \quad [IV.14]$$

where $M=29$ g/mol, s^2 is the collision diameter = 3.617 for air and Ω_m is the Lennard

Jones collision integral

$$\Omega_m = \frac{1.16145}{T^{*0.14874}} + \frac{0.52487}{\exp(0.7732T^*)} + \frac{2.16178}{\exp(2.43787T^*)} = 1.016$$

where, $T^* = \frac{kT_{ave}}{e} = 1.15$ and for air $\frac{e}{k} = 97$, from Table.E.1 (Bird et al., 2002).

Substituting in Eq. IV.14, the resulting μ was 0.01927 g/m-s. The air velocity (v) was computed using Eq. IV.15 for an AF=60 m³/hr.

$$\dot{v} = \frac{AirFlow}{area} \quad [IV.15]$$

$$AF = \frac{60 m^3/hr}{3600 sec} = 0.0166 \frac{m^3}{s}$$

$$\dot{v} = \frac{0.0166 m^3/s}{\frac{3.14}{4} * (0.106)^2 m^2} = 1.88 m/s$$

The density of air (ρ_{air}) was computed using Eq. IV.16 assuming ideal gas behavior.

$$\mathbf{r}_{air} = \frac{P * MW}{R * T_{ave}} \quad [IV.16]$$

$$\mathbf{r}_{air} = \frac{101325 \frac{N}{m^2} * 29 \frac{g}{mol}}{8.314 \frac{J}{molK} * 320.90 K} = 1101.37 \frac{g}{m^3}$$

Therefore, the Re number was

$$Re = \frac{d \dot{v} \mathbf{r}_{air}}{\mu} = \frac{0.106 m * 1.88 \frac{m}{s} * 1101.37 \frac{g}{m^3}}{0.01927 \frac{g}{ms}} = 1.114 E5$$

The Sc number was also calculated with previous results

$$Sc = \frac{\mu}{D_{AB} * \mathbf{r}} = \frac{0.0001927 \frac{g}{cms}}{0.2425 \frac{cm^2}{s} * 0.001101 \frac{g}{cm^3}} = 0.722$$

All the calculated values of Sh , Re and Sc are summarized in Table IV.5 for the operating conditions of $AF=60 \text{ m}^3/\text{hr}$ and $T=60^\circ\text{C}$ for the falling rate period. The same procedure was employed to determine the dimensionless number of Sh , Sc and Re for the other operating conditions.

Table IV.5. Results of Sc , Re and Sh numbers for $AF=60 \text{ m}^3/\text{hr}$ and $T=60^\circ\text{C}$ in the falling rate period

Time (min)	Sc	Re	Sh
9	0.7227	1.157E+05	9.931
12	0.7396	1.148E+05	9.145
15	0.7516	1.136E+05	7.843
18	0.7537	1.130E+05	7.532
21	0.7546	1.125E+05	6.666
24	0.7508	1.118E+05	6.259
27	0.7529	1.111E+05	5.607
30	0.7527	1.108E+05	5.367

An average number of each Sc , Sh and Re were calculated for both periods for each operating condition. After determining the average values of Sc , Sh and Re for all runs, the empirical correlation was developed.

The sample calculation presented below correspond to the falling rate period for operating conditions of $AF=40, 50$ and $60 \text{ m}^3/\text{hr}$, and $T=60$ and 80°C (AF1). Table IV.6 presents the total average number of Sc , Sh and Re for AF1. To calculate the average total dimensionless numbers, Eq. IV.16 was used.

$$\overline{Sc} = \frac{\sum Sc_{in \text{ fallingrate}}}{\text{total number of } Sc} \quad [IV.16]$$

A sample calculation for \overline{Sc} number is illustrated below. Similar calculations were done for the other dimensionless numbers.

$$\overline{Sc} = \frac{0.7553 + 0.7396 + 0.7516 + 0.7537 + 0.7546 + 0.75080 + .7529 + 0.7527}{8} = 0.751$$

Table IV.6. Results of \overline{Sc} , \overline{Re} and \overline{Sh} numbers for AF1

Operating Conditions	\overline{Sc}	\overline{Sh}	\overline{Re}
AF 40 T80	0.726	4.470	6.952E+04
AF 40 T60	0.784	4.032	7.424E+04
AF 50 T60	0.774	5.752	9.335E+04
AF 50 T80	0.717	6.306	8.734E+04
AF 60 T80	0.713	6.831	1.046E+05
AF 60 T60	0.751	7.293	1.123E+05

After determining the dimensionless numbers: \overline{Sc} , \overline{Re} and \overline{Sh} numbers, for each set of operating conditions, the values were analyzed applying a non linear regression method (LM). An example of the results provided from the commercial software at AF1 is shown below.

Employed Method: Nonlinear regression (L-M)

Model: $Sh = A*(Sc^b)*(Re^c)$

Variable	Initial guess	Value	95% confidence
A	5.0E-04	7.131E-05	1.644E-04
B	-1	- 1.1105649	2.4673246
C	0.8	0.9627194	0.1981432

NOTE: Calculations exceeded the maximum number of iterations.

Nonlinear regression settings

Max # iterations = 64

Precision

R^2 = 0.9179165

R^2_{adj} = 0.8631942

Rmsd = 0.1387551

Variance = 0.2310356

General

Sample size = 6
 # Model vars = 3
 # Indep vars = 2
 # Iterations = 64

Therefore, a specific empirical correlation for AF1 was developed to determine the $k_g a$ for the falling rate period as shown in Eq. IV.17.

$$Sh = 7.131E - 05 * Sc^{-1.1105} * Re^{0.9627}$$

$$k_g a = 7.131E - 05 * Sc^{-1.1105} * Re^{0.9627} \left(\frac{D_{AB}}{d} \right) \quad [IV.17]$$

Similar calculations were done for the constant rate period for AF1 and for both periods for AF 2. Table IV.7 shows the results of the parameters found for the empirical correlations for AF1 and AF2.

Table IV.7. Results of parameters of the empirical correlations for AF1 and AF2

Period	a	b	c
Constant rate AF1	1.02E-10	-2.82	2.28
Constant rate AF2	3.20 E-06	-2.33	1.35
Falling rate AF1	7.13E-05	-1.11	0.96
Falling rate AF2	5.61E-07	0.295	1.43

IV.4 Prediction of moisture content

Eq. IV.17 was then used to estimate the $k_g a$ at different operating conditions of AF 1 in the falling rate period. For AF=60 m³/hr and T=60 °C at 12 minutes, the predicted value is

$$k_g a = 7.131E - 05 * (0.7396^{-1.1105}) * (113790.4502^{0.9627}) * \left(\frac{0.2439 \frac{cm^2}{s}}{10.6cm} \right) = 0.203 \text{ cm/s}$$

Changing the units of $k_g a$, (as shown in section IV.3), the new value is 0.0179 kg/s. The MC (w_p) was then predicted using Eq. II.4.

$$w_p = \frac{6.0\% * 0.60716 \frac{mol}{s} * 29.31 \frac{J}{molK}}{0.01786 \frac{kg}{s} * 950 \frac{J}{kgK}} \ln \left(\frac{61.72^\circ C - 18.73^\circ C}{35.64^\circ C - 18.47^\circ C} \right) = 5.810\% MC$$

The residual of MC was evaluated using Eq. IV.18.

$$\text{Residual} = \left| MC_{\text{experimental}} - MC_{\text{predicted}} \right| \quad [\text{IV.18}]$$

$$\text{Residual} = \left| 5.61\% - 5.81\% \right| = 0.200\%$$

Similar calculations were performed for the other operating conditions, as well as for the varying composition experiments. In the latter, the data used corresponded to Formulation 2 and 3 (See Chap. III). The results for all experiments are discussed in Chapter V

CHAPTER V. RESULTS AND DISCUSSION

V.1 Experimental Design

The Split Plot Experimental Design (SPED) was employed to define the required experiments for the determination of the empirical correlation. This methodology was chosen because the sample collected came from the same batch (1 kg) in the FBD and it reduces the number of observations allowing equal statistical analysis as in factorial design. (Montgomery (1996))

The factors considered in this study were drying time, air flow (AF) and drying temperature (T). Table V.1 shows the operating conditions of the experimental design. As can be seen, the SPED depends on five (5) air flows at two (2) temperatures with 11 different intervals of time. The mass load (1 kg) and the initial MC (~9-10% w/w) were constant for all runs.

Table V.1. Experimental design variables

AF (m ³ /hr)	T (°C)
40	60,80
50	60,80
60	60,80
70	60,80
80	60,80

The initial experiments used conditions of AF=40, 60 and 80 m³/hr at T=60 and 80 °C. Under these conditions, the behaviors of the three drying curves were different. Figure

V.1 depicts the drying curves $AF=40, 60$ and $80 \text{ m}^3/\text{hr}$ at $T=60^\circ\text{C}$. $AF=40$ depicts a constant rate period for almost the drying time, while $AF=80$ depicts a falling rate period for most of the entire drying time, and $AF=60$ depicts clearly the two regions. For smallest AF , the interactions between the particles are less and the collisions have a small impact. Thus, the drying is dominated solely by evaporation. This behavior depicts a low increment in T and the granulation tends to dry with large drying time. For the largest AF , the behavior is different because the collisions cause more friction and the drag of water. More friction causes the T at the interface to increase and thus the driving force for mass transfer. Therefore, the mass transfer increases, and the drying time is reduced according to Chen *et. al.* (1999).

The behavior of each curve is totally different from the others, thus additional data were needed to have a better understanding of the drying experiments. Therefore, to develop the empirical correlation, additional experiments were performed at operating conditions of $AF=50$ and $70 \text{ m}^3/\text{hr}$ at $T=60$ and 80°C .

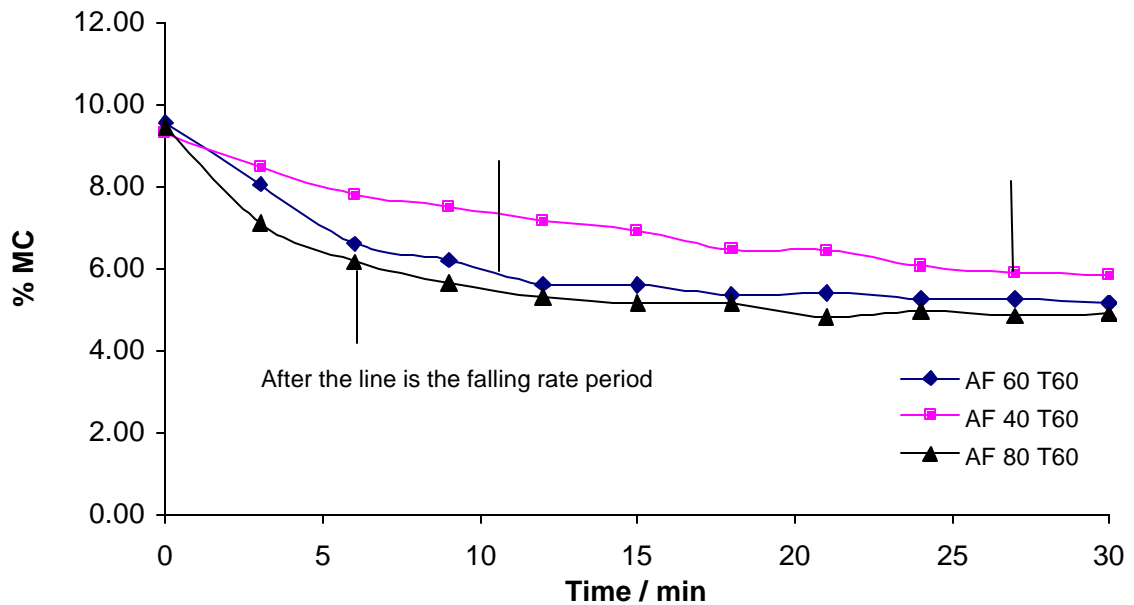


Figure V.1. Drying curves for AF=40, 60 and 80 m³/hr at T=60°C

Figure V.2 shows the drying curve for AF=40, 50, 60, 70 and 80 m³/hr at T=60 °C. For high AF, the drying time was reduced to 15 minutes as shown in the figure. As mentioned before, at high AF, the fluidizations have a very high velocity and the interaction between the particles increase dramatically. This could cause more friction and an increase in the mass transfer.

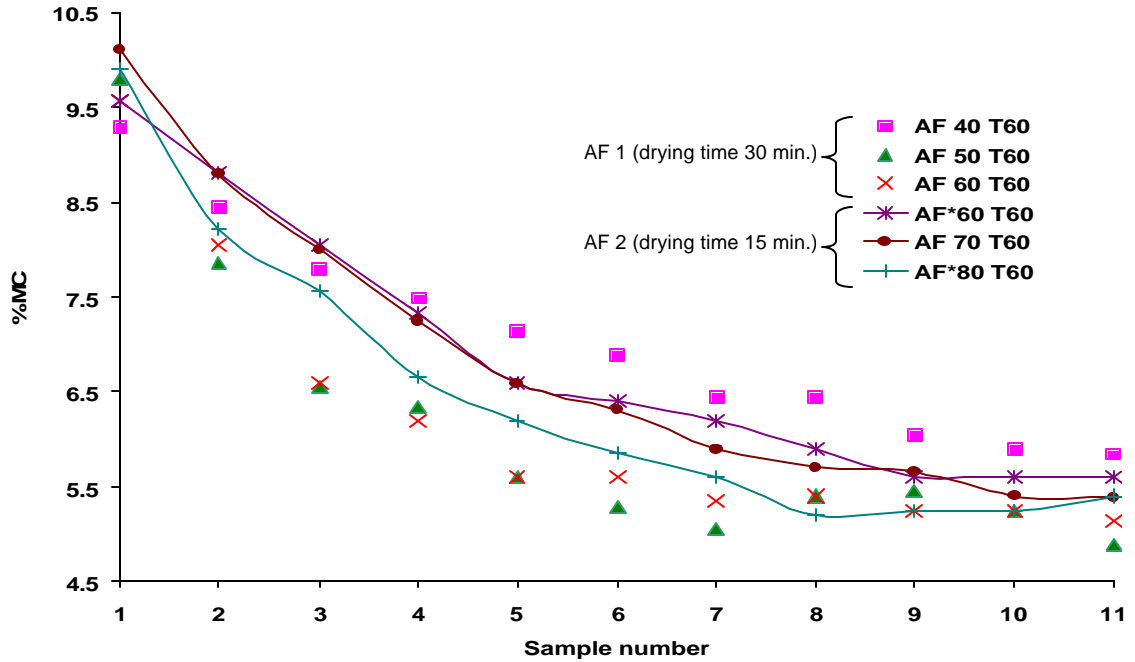


Figure V.2. Drying curves for AF=40, 50, 60, 70 and 80 m³/hr at T=60°C

Based on the different behavior of the six drying curves, as can be seen in Fig. V.2, the data were divided in two sets. As mentioned above, each set is governed by different phenomena that are difficult to be included in one correlation. Thus, this non linear behavior was modeled by two different correlations. One correlation for AF=40, 50 and 60 m³/hr (AF1) and other with AF =60*, 70, and 80 m³/hr (AF2) at T=60 and 80 °C (* Replicates with different intervals of time). The operating condition of AF=60 m³/hr was used for both regions since its drying curve presents both phases very well.

The empirical correlations of the mass transfer coefficients

Figure V.3 includes the computed $k_g a$ for the constant rate period. The values of $k_g a$ increase with T , and the convective mass transfer rate reaches the maximum at this zone agreeing with the theory (Treybal, 1978). The graph indicates that the $k_g a$ values are constant for the evaporation rate zone for each operating conditions. As is seen in the

graph, all the values are close to 0.1 which are in close agreement with the values of 0.013 to 0.47 kg/s reported by Cussler (1984) for similar situations for water-air mass transfer processes such as humidification and evaporation. Similar behavior was found for the constant rate of AF2 where the average value was 0.095 kg/s.

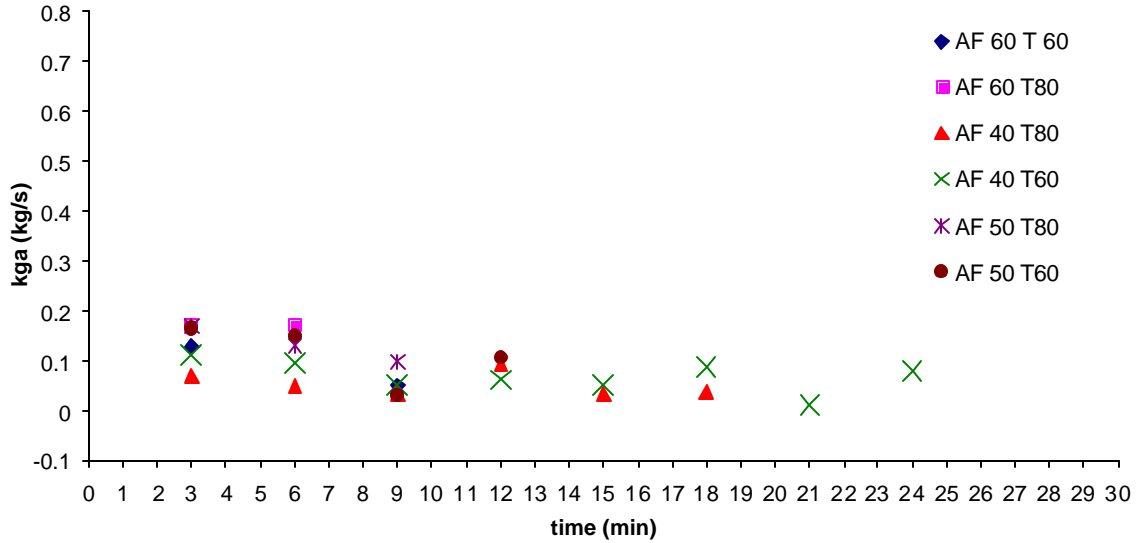


Figure V.3. Experimental mass transfer coefficient values for the constant rate period for AF1

Figure V.4 shows the experimental values of the k_ga for the falling rate period of AF1. At these conditions, the k_ga , as can be seen, is almost constant, with an average value of 0.015 kg/s. Comparing to Figure V.3, it can be observed that k_ga is greater in the constant rate period than in the falling rate period. In the constant rate period, the evaporation rate dominates and the k_ga increases more rapidly than in the falling rate period.

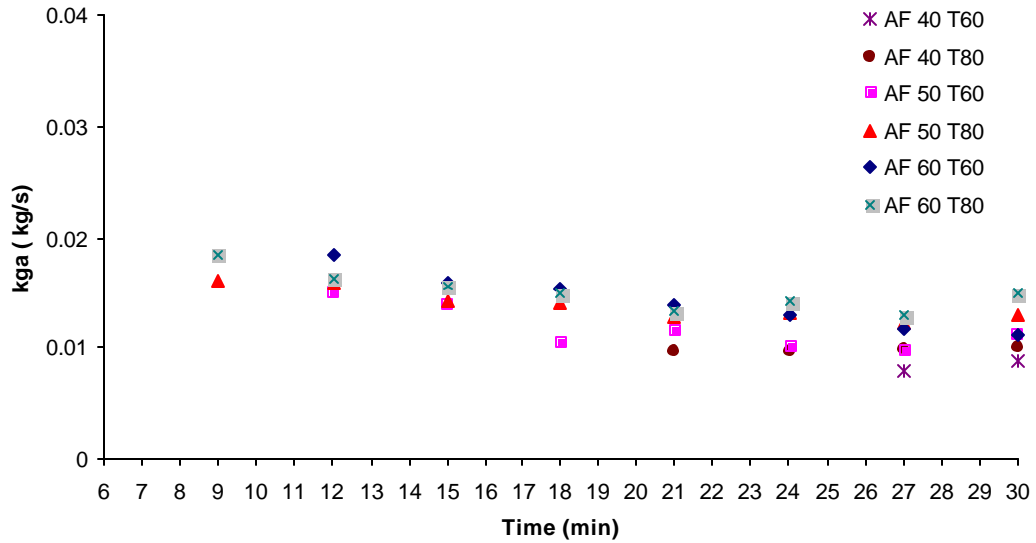


Figure V.4. Experimental mass transfer coefficient values for the falling rate period of AF 1

In the constant rate drying period, the surface of the solid is initially very wet and a continuous film of water exists on the drying surface. This water is entirely unbound, thus acting as if the solid were not present. The evaporation rates under the given air conditions are independent of the solid and is essentially the same as that of a free liquid surface.

From Figure V.4, it can also be seen that the final $k_g a$ is independent of the process parameters. This behavior can also be explained by the principle that at the beginning the mass transfer plays a main role in the constant rate but eventually the internal mechanism of diffusion displaces the convective mass transfer during the falling rate period.

Once the experimental values of $k_g a$ were calculated, the next step was to determine the dimensionless number groups of Sc , Sh and Re to obtain an empirical correlation, Fig. V.5 to V.10.

Sc values decreased with T which is in agreement with theory (Bennett *et al.*, 1982). In the other hand Sc increased with low air flows at constant temperature, except for the constant rate of AF1. This exception may occur because the interactions between particles-particles are low at small air flow. On the other hand, as the air velocity increases, T increases too due to the collision of particle thus causing a decrease in Sc . For the falling rate period, the behavior is different despite the air flow in the same, due to the continuous increase in temperature at this zone.

During the drying process, heat and water evaporation must pass through a static gas film between the granule surface and air when heat is transferred from air to granules, or vapor is transferred from granules to air, respectively. Only by decreasing the gas film thickness heat and mass transfer resistances can be decreased, thus heat and mass exchange are enhanced. When the gas velocity is increased, the collisions between particles are intensified, so that the static gas film becomes thinner and burst frequently. At the end, mass transfer is enhanced.

As can be seen in Fig. V.7 and V.8, the Re number decrease with high T while increases with high AF for both stages. Therefore, the mass transfer coefficient increases with greater Re .

The data obtained provides evidence that the behavior of the curves of Sh depends on the operating conditions and the period. For examples, at the constant rate period for AF1, Sh decrease as T increases while for AF2, and the same period, Sh increase proportionally with T . At the latter condition, not all the water goes through evaporation but rather removed by a drag-like phenomenon (Fig. V.9 and V.10).

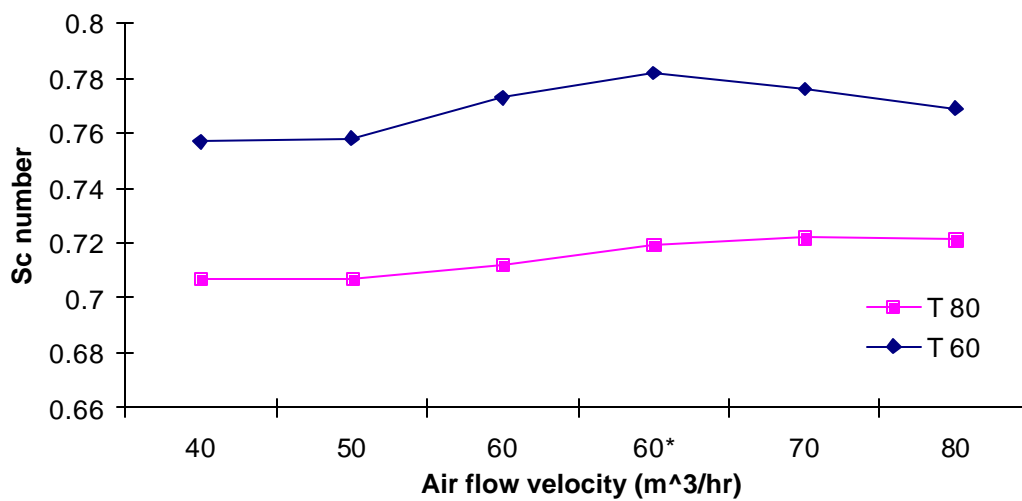


Figure V.5. *Sc* number as a function of air velocity for the constant rate period

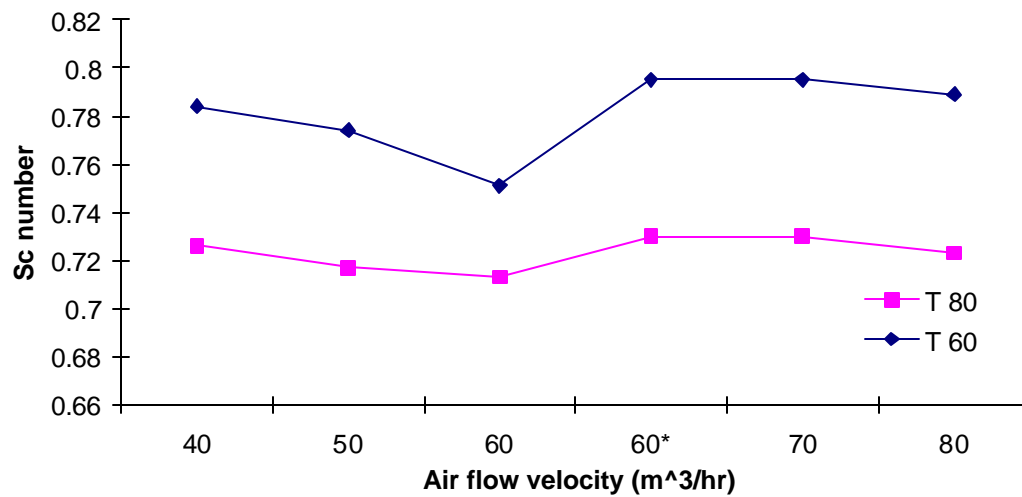


Figure V.6. *Sc* number as a function of air velocity for the falling rate period

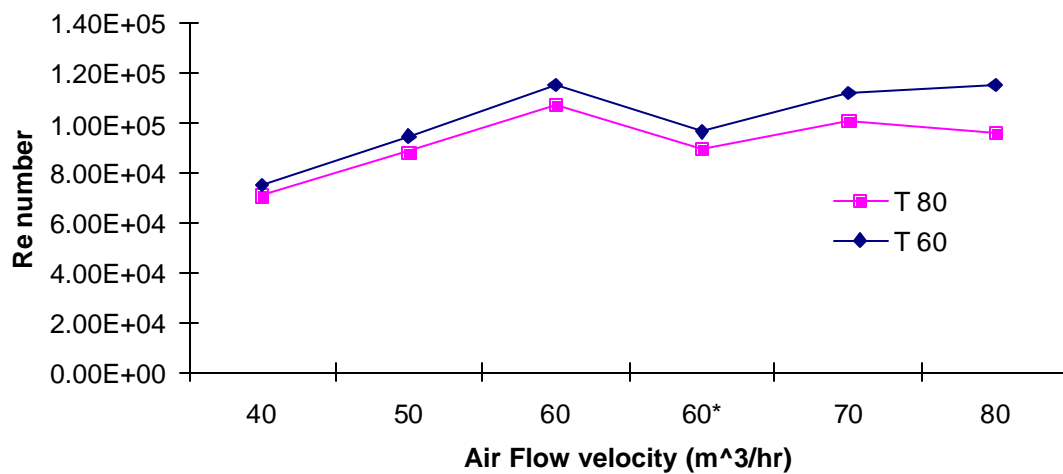


Figure V.7. Re number as a function of air velocity for the constant rate period

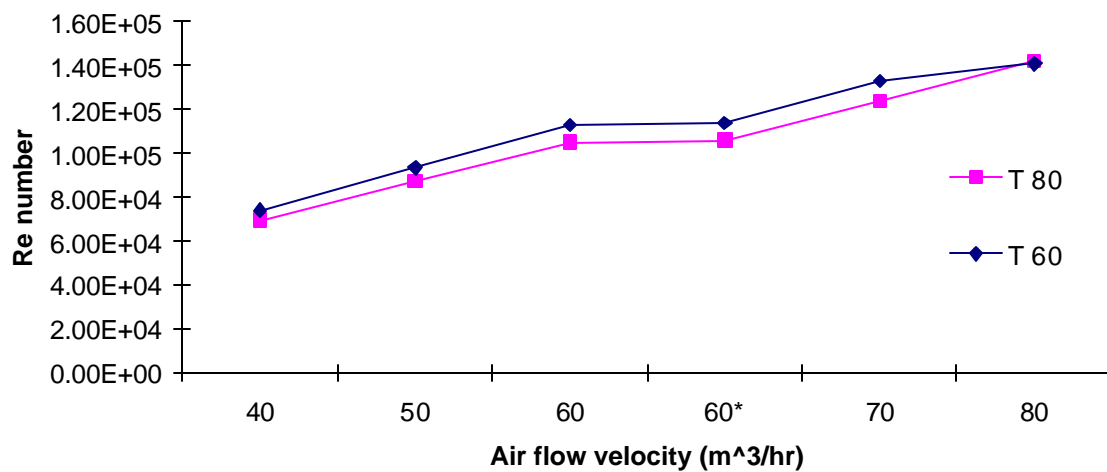


Figure V.8. Re number as a function of air velocity for the falling rate period

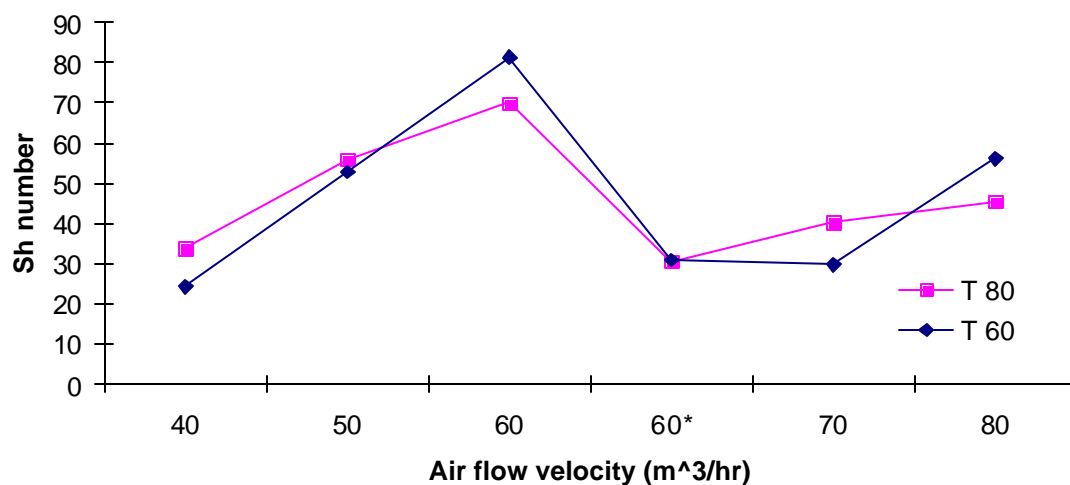


Figure V.9. *Sh* number as a function of air velocity for the constant rate period

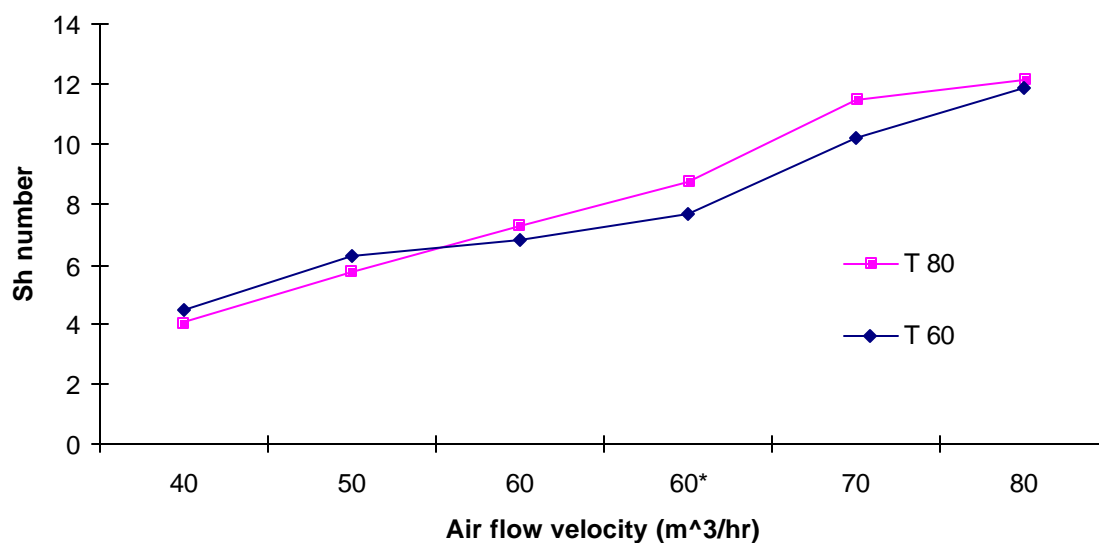


Figure V.10. *Sh* number as a function of air velocity for the falling rate period

Table V.2 includes the results obtained for the adjusting parameters and the statistics. According to the results, the variances were smaller for the falling rate than for the constant rate for both sets of operating conditions.

The obtained results of the corresponding adjusting parameters show that T have a strong influence in Sc number. The corresponding adjusting parameter values (c) indicate that air velocity has the largest influence in Sh since it obtained positive and the highest values.

As can also be seen from the table, the temperature and air flow velocity have similar weight in the coefficient value for the constant rate region. The same is true for the falling rate period but with a smaller weight than in previous region. In the falling rate zone, the diffusion is a strong function of T , thus dominates this section.

The constant a , emphasizes the non linear behavior of the drying process as a function of air flow velocity and drying temperature.

Table V.2. Results of empirical correlation parameters and statistic analysis for AF 1 and AF 2

Period	a	b	c	s	R²	RMSD
Constant rate AF1	1.02E-10	-2.82	2.28	42.415	0.945	1.880
Constant rate AF2	3.20 E-06	-2.33	1.35	156.527	0.169	3.612
Falling rate AF1	7.13E-05	-1.11	0.96	0.231	0.918	0.139
Falling rate AF2	5.61E-07	0.295	1.43	0.0913	0.983	0.0872

Figures V.11 to V.14 show the results of predicted of the $k_g a$ for AF1 and AF2. As can be seen from all the figures, the predicted values of $k_g a$ are in very close agreement with the experimental ones. The rule of thumb to either accept or reject the prediction establish that error should be 30 % or less (Treybal (1978), Kneule (1966), and Bennett (1982)). All the prediction of $k_g a$ had 30 % except for the constant rate of AF2 run.

Figure V.13 depicts the $k_g a$ prediction for the constant rate period for AF2. The curve for $T=80 \text{ m}^3/\text{hr}$ indicates a large deviation between experimental and predicted results with the highest error was 40 % for the condition of $AF=70 \text{ m}^3/\text{hr}$. Moreover, as seen in the graph, the predicted $k_g a$ value for $AF=80$ depicts a large deviation too, but less than 30%. Furthermore, as is shown in the MC curves, the predictions are very well at these conditions. The reason for the behavior of the predicted $k_g a$ at these conditions could be due to the high velocity and the sampling method. The non homogeneous fluidization could have lead to segregation during the sampling, what could have led to high variation in the MC. This in term could have led to the high variation in $k_g a$. The non uniform drying of the powders due to the fluidization could have also played a big role in the no monotonic behavior of $k_g a$.

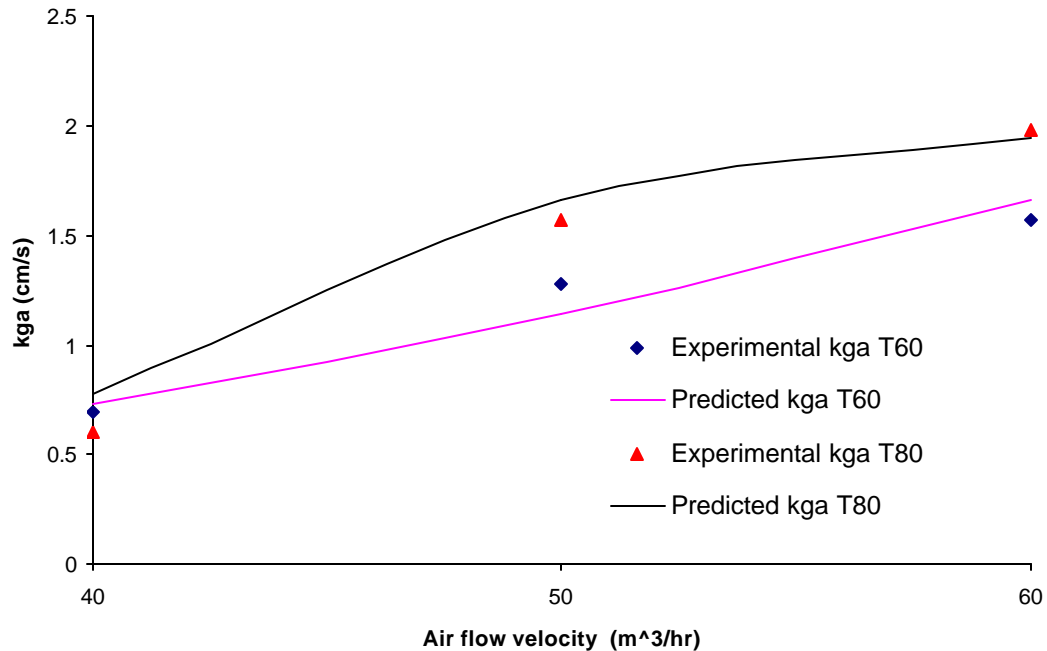


Figure V.11. Comparison of experimental and predicted $k_g a$ for the constant rate period (AF1)

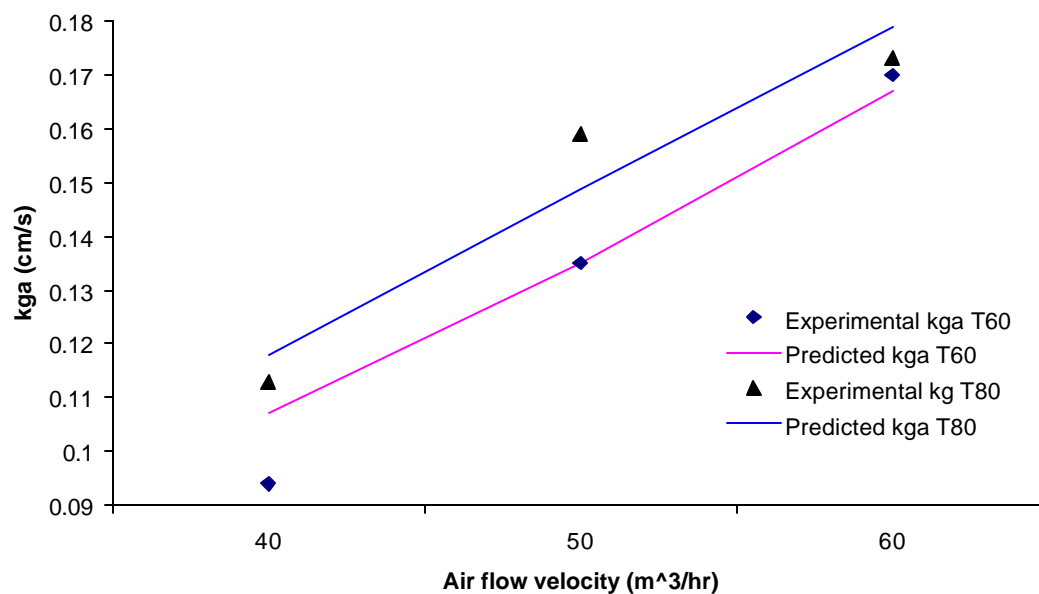


Figure V.12. Comparison of experimental and predicted k_{ga} for the falling rate period (AF1)

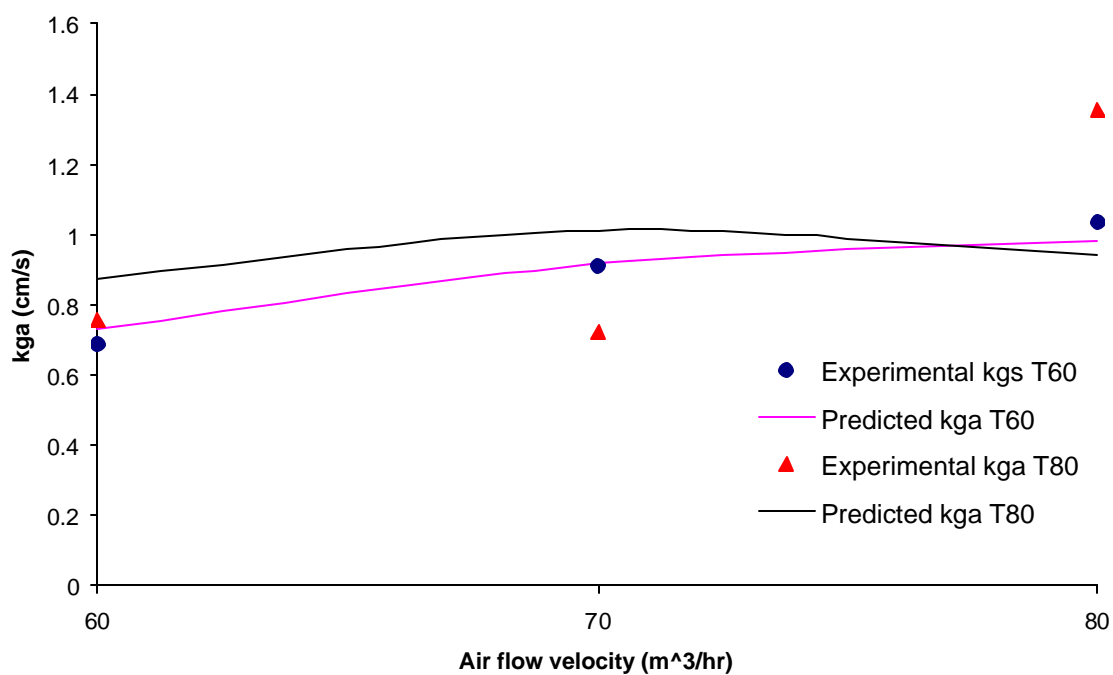


Figure V.13. Comparison of experimental and predicted k_{ga} for the constant rate period (AF2)

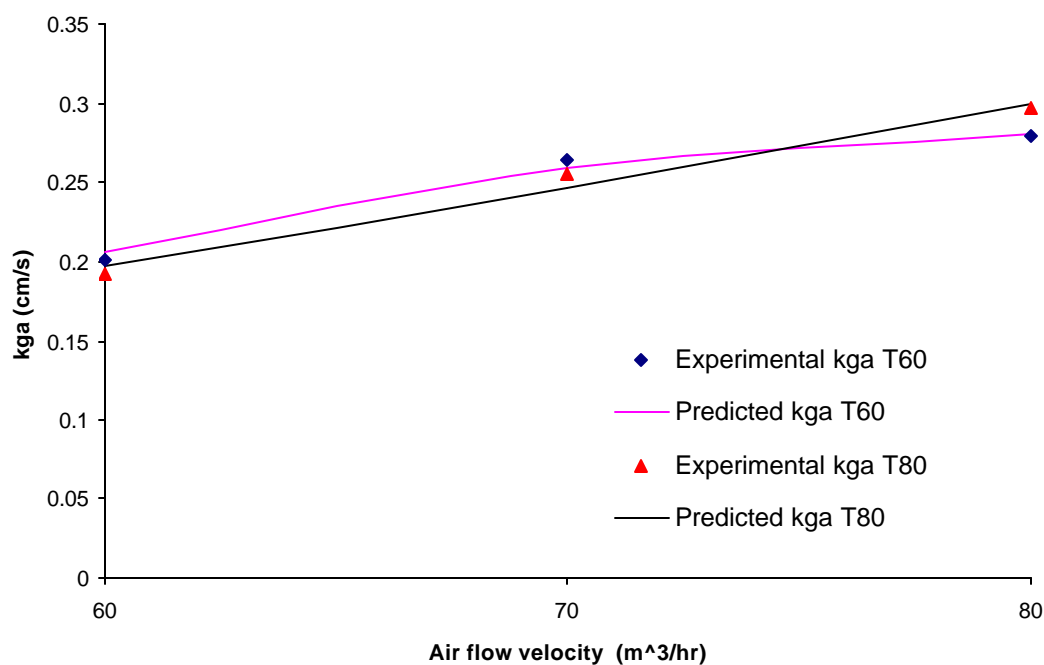


Figure V.14. Comparison of experimental and predicted k_{ga} for the falling rate period (AF2)

V.3 Prediction of moisture content

Figures V.15 to V.20 depict the prediction of the drying curves. As a rule of thumb, the residuals between predicted and actual values have to be lower than 1% to either accept or reject an empirical correlation base on pharmaceutical industrial batch record. The obtained results for the prediction of MC were lower than 1%. This demonstrates that the dimensionless group chosen contains the critical parameters to predict the mass transfer in a drying process.

From these graphs, it can be seen that the correlation of k_{ga} produced a suitable prediction for the MC at the constant rate period for AF1 conditions. Additional drying curves results are presented in Appendix C, D and E, where in general, all curves depict similar behaviors with a mean values less than 1%.

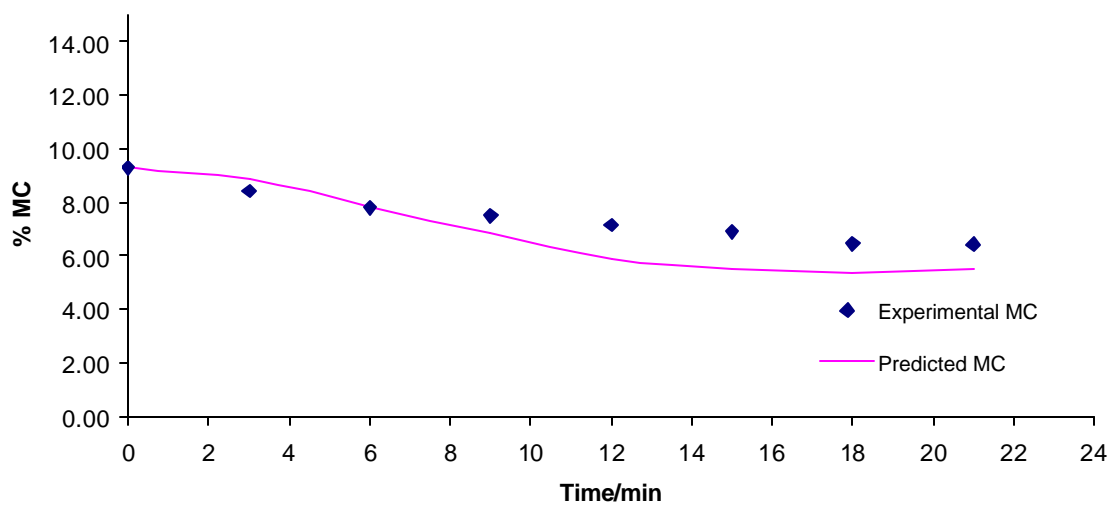


Figure V.15. Moisture content prediction for the constant rate period at $AF=40 \text{ m}^3/\text{hr}$ and $T=60^\circ\text{C}$

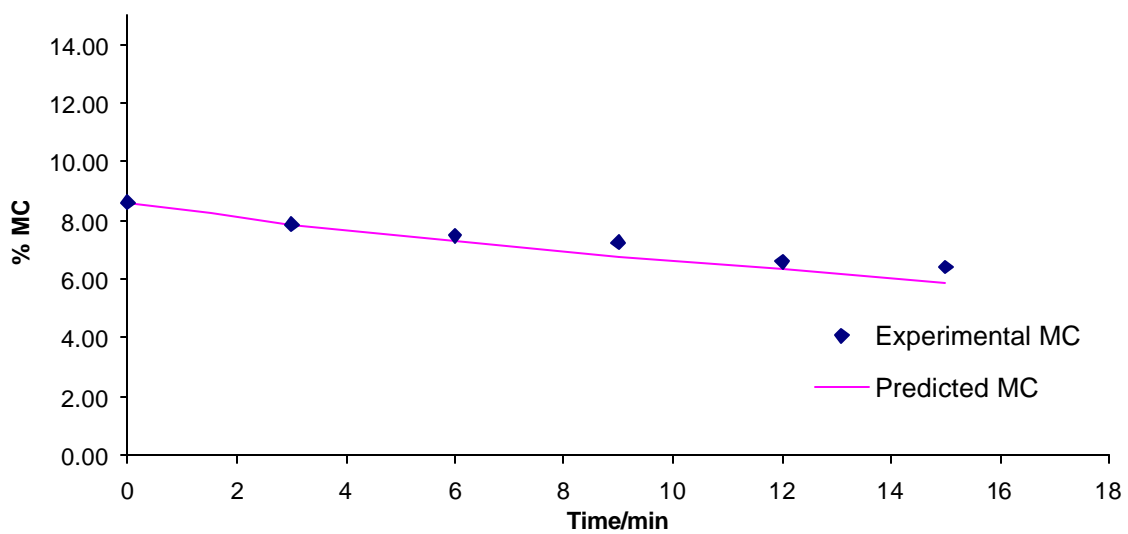


Figure V.16. Moisture content prediction for the constant rate period at $AF=40 \text{ m}^3/\text{hr}$ and $T=80^\circ\text{C}$

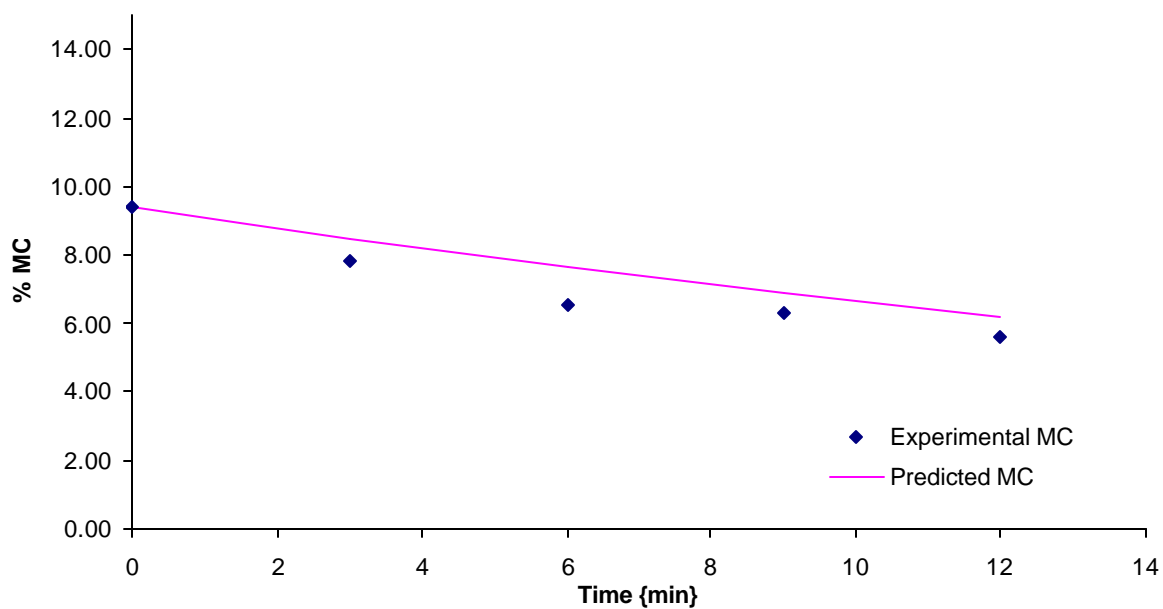


Figure V.17. Moisture content prediction for the constant rate period at $AF=50 \text{ m}^3/\text{hr}$ and $T=60^\circ\text{C}$

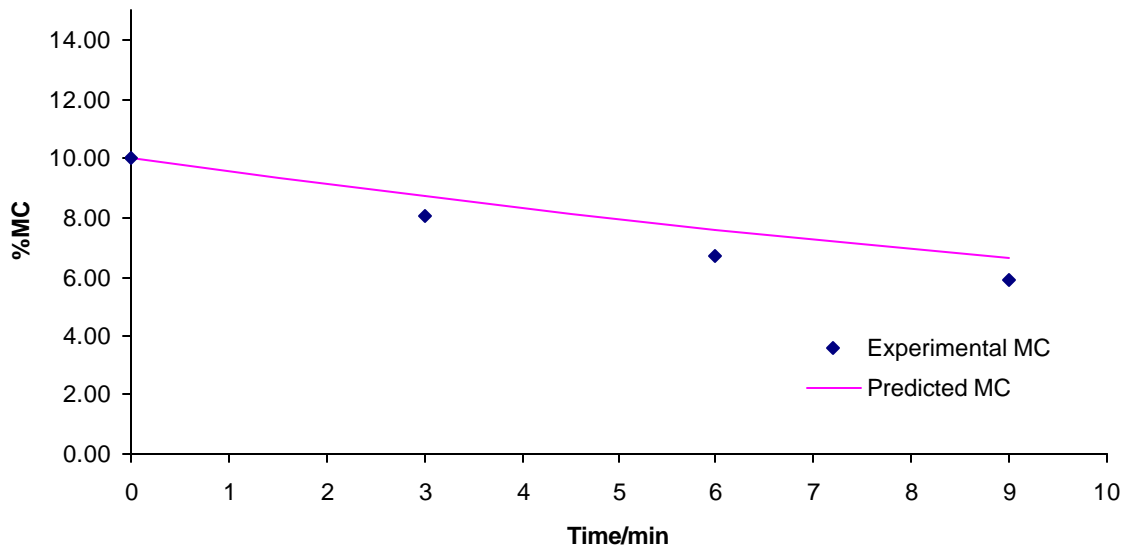


Figure V.18. Moisture content prediction for the constant rate period at $AF=50 \text{ m}^3/\text{hr}$ and $T=80^\circ\text{C}$

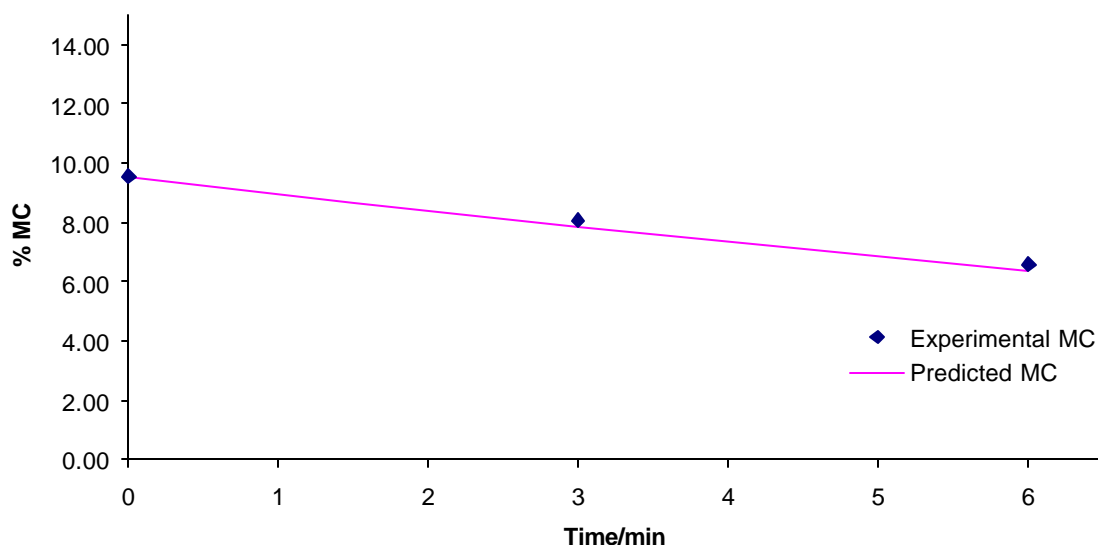


Figure V.19. Moisture content prediction for the constant rate period at $AF=60 \text{ m}^3/\text{hr}$ and $T=60 \text{ }^\circ\text{C}$

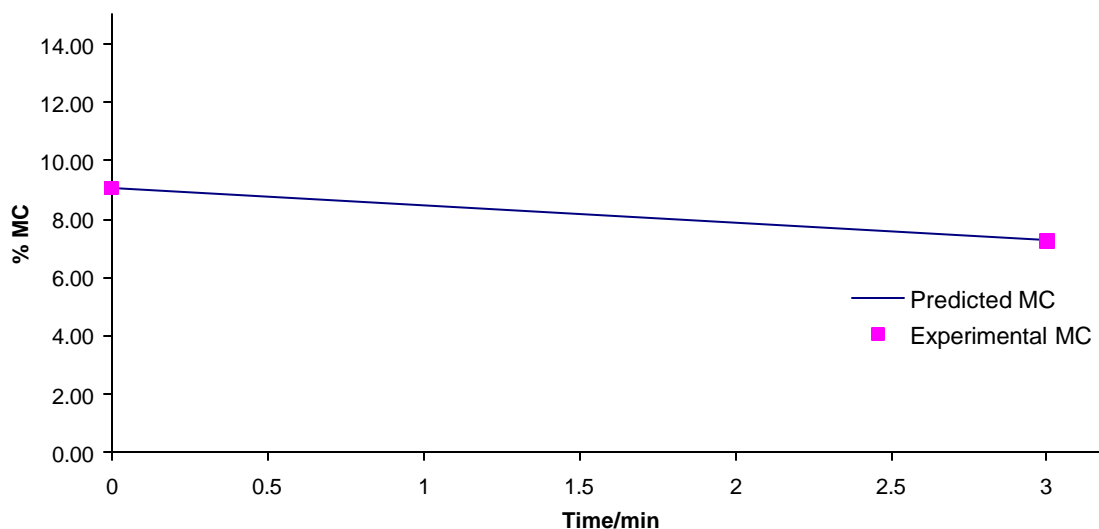


Figure V.20. Moisture content prediction for the constant rate period at $AF=60 \text{ m}^3/\text{hr}$ and $T=80 \text{ }^\circ\text{C}$

Figure V.21 depicts the moisture content prediction for the constant rate period for AF2 condition. The $k_g a$ predictions for this region produced an error over 30% as shown Fig. V.13. However, as seen in Fig. V.21, the MC residual between the predicted values and experimental was less than 1%, indicating a suitable prediction too. Similar results were found for the other runs for these conditions (See Appendix D).

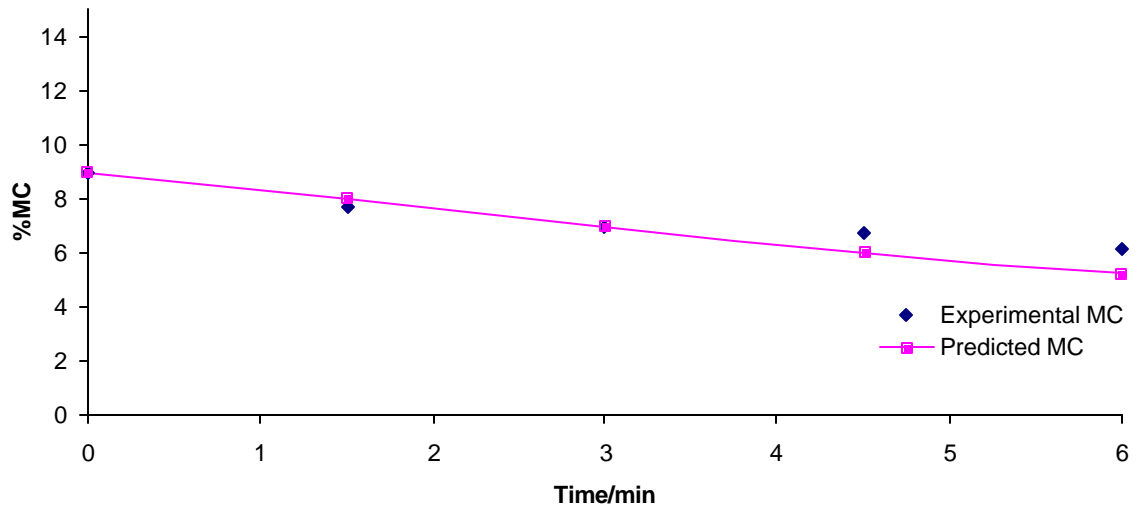


Figure V.21. Moisture content prediction for the constant rate period at $AF=70 \text{ m}^3/\text{hr}$ and $T=80^\circ\text{C}$

V.4 Varying composition experiments

The empirical correlations were validated with experiments varying the composition of the granulation (Table III.1). Figures V.22 to V.26 depict the prediction of the empirical correlations for the varying composition experiments using granulation 2. As can be observed, the prediction accuracy follows the trends obtained for granulation 1. The residual results for all runs were less than 1 %, too.

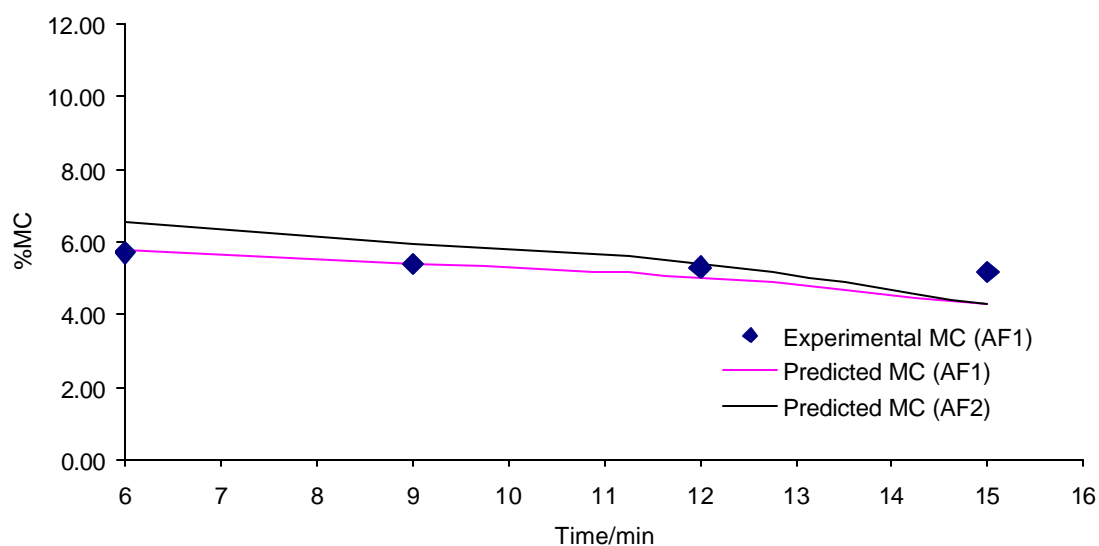


Figure V.22. Moisture content prediction for the falling rate period of the varying composition experiments at $AF=60 \text{ m}^3/\text{hr}$ and $T=80^\circ\text{C}$

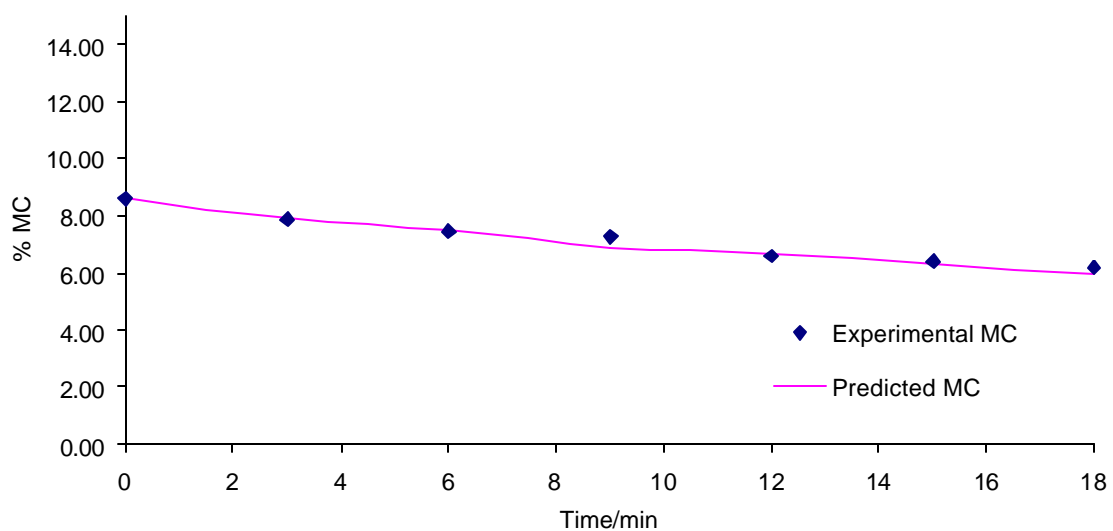


Figure V.23. Moisture content prediction for the constant rate period of the varying composition experiments at $AF=40 \text{ m}^3/\text{hr}$ and $T=80^\circ\text{C}$

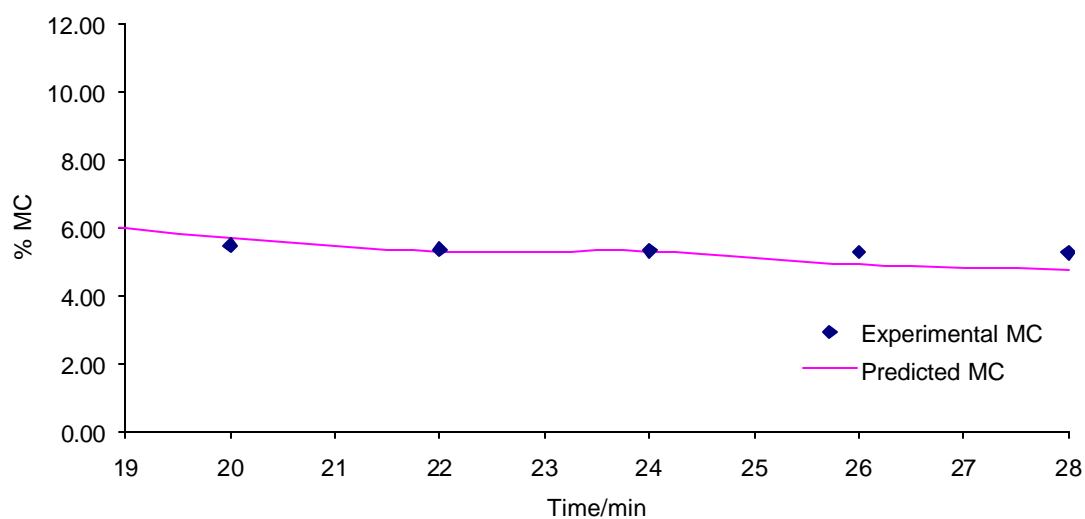


Figure V.24. Moisture content prediction for the falling rate period of the varying composition experiments at $AF=40 \text{ m}^3/\text{hr}$ and $T=80^\circ\text{C}$

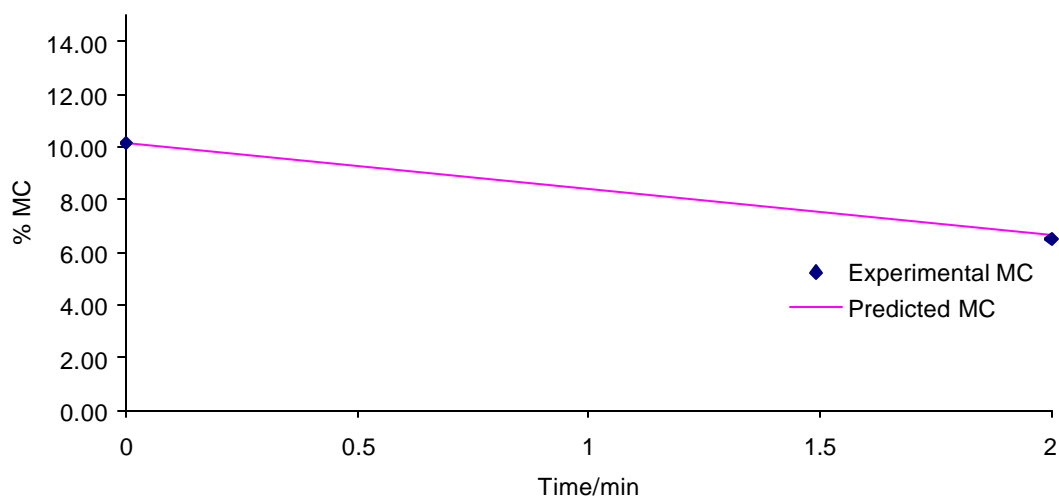


Figure V.25. Moisture content prediction for the constant rate period of the varying composition experiments at $AF=80 \text{ m}^3/\text{hr}$ and $T=80^\circ\text{C}$

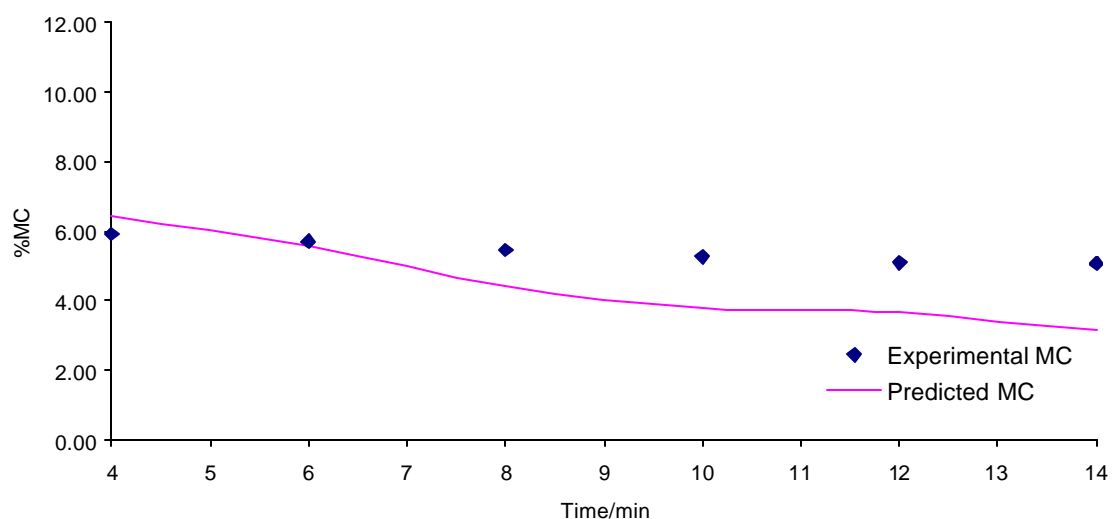


Figure V.26. Moisture content prediction for the falling rate period of the varying composition experiments at $AF=80 \text{ m}^3/\text{hr}$ and $T=80^\circ\text{C}$

The results show that a change in material composition had little influence in the empirical correlation. As shown in the graphs, granulations 1 and 2 seem to have similar behavior and morphology. For granulation 1, the particle size distribution of the granulations were 248.92 to 63.5 μm (see Fig. V.27). Comparing to granulation 2, the particle size distribution was 248.92 to 104.14 μm (see Fig. V.28). The difference in particle size was considerably for both granulations. Moreover, the lactose monohydrate for granulation 1 had a particle diameter between 63 and 400 μm , and for granulation 2 has a range between 74 to 595 μm . The particle size distribution was difference in each ingredient. Therefore, this difference could affect the $k_g a$ prediction due to the transfer area between particles, and subsequently the prediction of the drying curves. As can be seen in the curves, this was not the case and the predictions of MC were suitable.

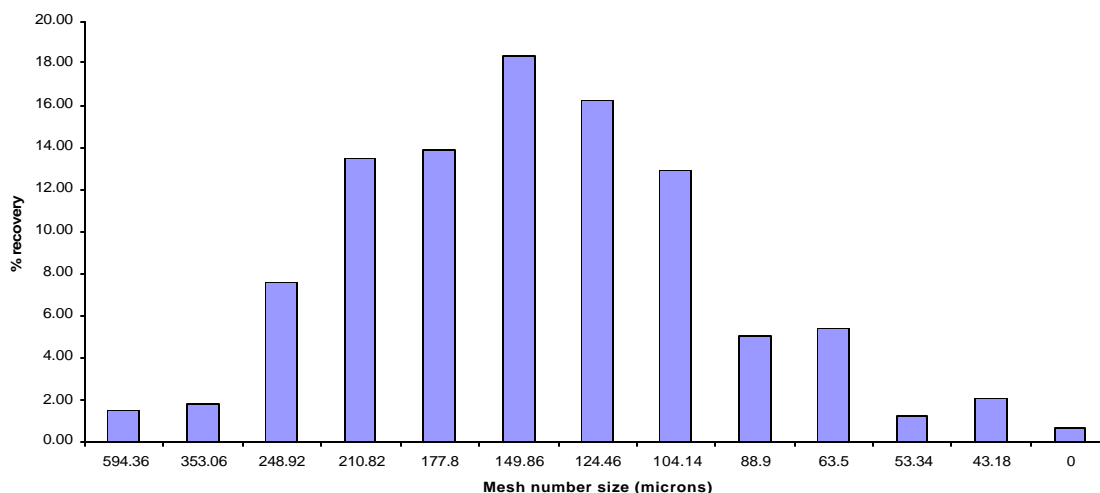


Figure V.27. Particle size distribution for granulation 1

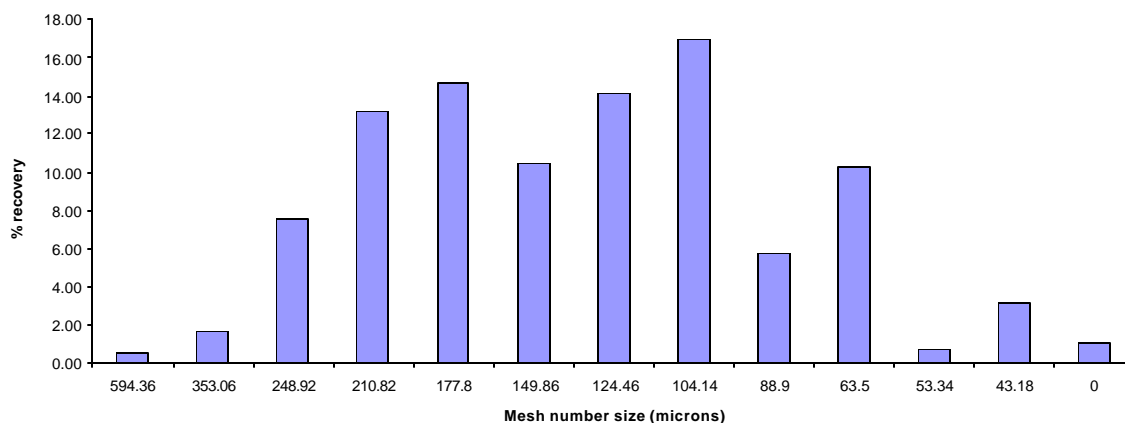


Figure V.28. Particle size distribution for granulation 2

The chemistry of both lactoses (granulac 70 and spray dryer) seems not to affect the prediction of final moisture content. Especially for this set of experiments, the differences in lactose had little influence in the mass transfer and both granulations seem to have a little difference in behaviors. Hence, the chemistry of the powders used seems to have small influence in the drying demonstrating that using only parameters such as temperature and air flow velocity is sufficient.

Other experiments were conducted using Formulation 3. Comparing granulation 1 to 3, the third one has lactose anhydrous. The difference in properties between the anhydrous and lactose monohydrate is the molecular water bond in the monohydrate. Another difference was the particle diameter in the lactose anhydrous. The range of the particle size for lactose anhydrous was 74 to 250 μm . For granulation 1 and 3 the quantity of water was different. The lactose anhydrous has more water than the monohydrated water. The particle size distribution of granulation 3 was different comparing to granulation 1 and 2 (see Fig. V.32). The size range was 248.92 to 177.8 μm , where the granules are bigger to other granulations. The behavior of the granulations in terms of drying seems to be similar than in granulation 1. Figure V.29 to V.31 depict the drying curves for the experiment varying composition for granulation 3. As can be seen in the graph, the behavior is similar and the final MC predictions are suitable. In addition, the particle size does not represent a strong factor for granulation 3 comparing to T and AF. Therefore, the developed empirical correlation can predict the MC for granulation with similar ingredients even if a small difference in particle size distribution exists. For granulation 2 and 3, the average residuals MC was less than 1%.

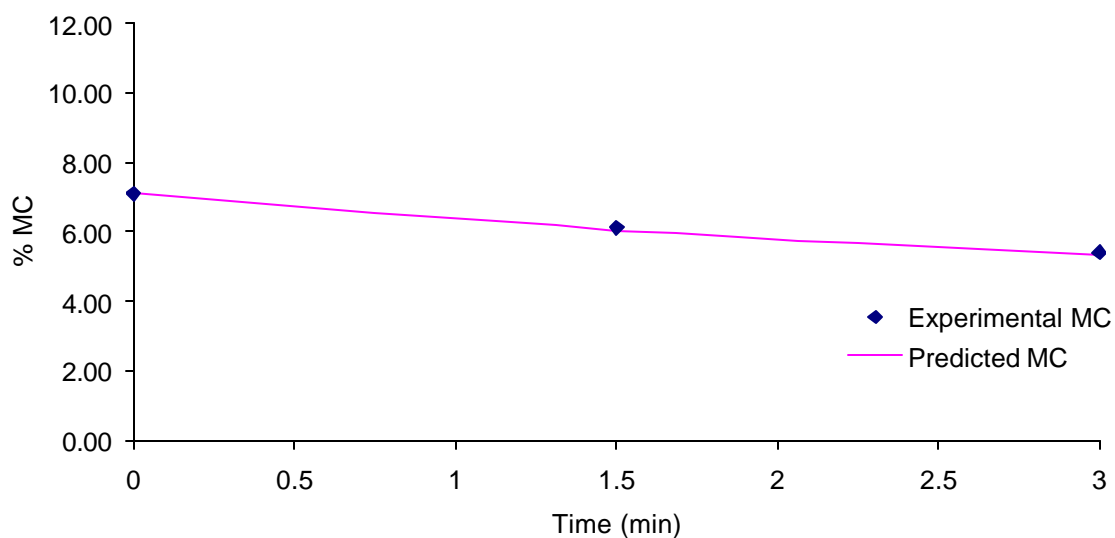


Figure V.29. Moisture content prediction for the constant rate period of the varying composition experiments at $AF=80 \text{ m}^3/\text{hr}$ and $T=60 \text{ }^\circ\text{C}$ (Formulation3)

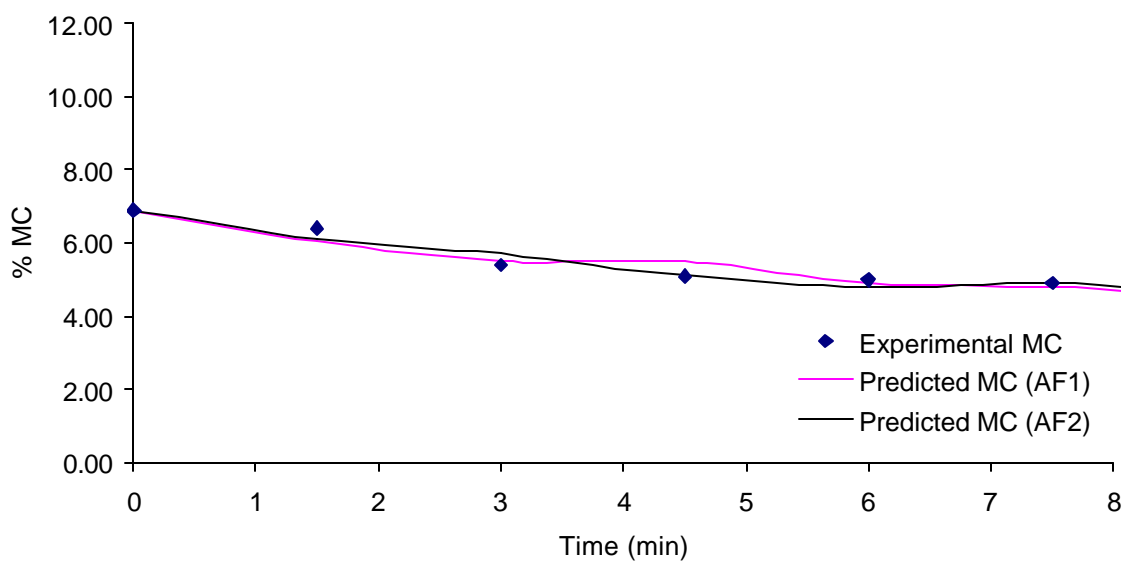


Figure V.30. Moisture content prediction for the constant rate period of the varying composition experiments at $AF=60 \text{ m}^3/\text{hr}$ and $T=60 \text{ }^\circ\text{C}$ (Formulation3) using correlations AF1 and AF2

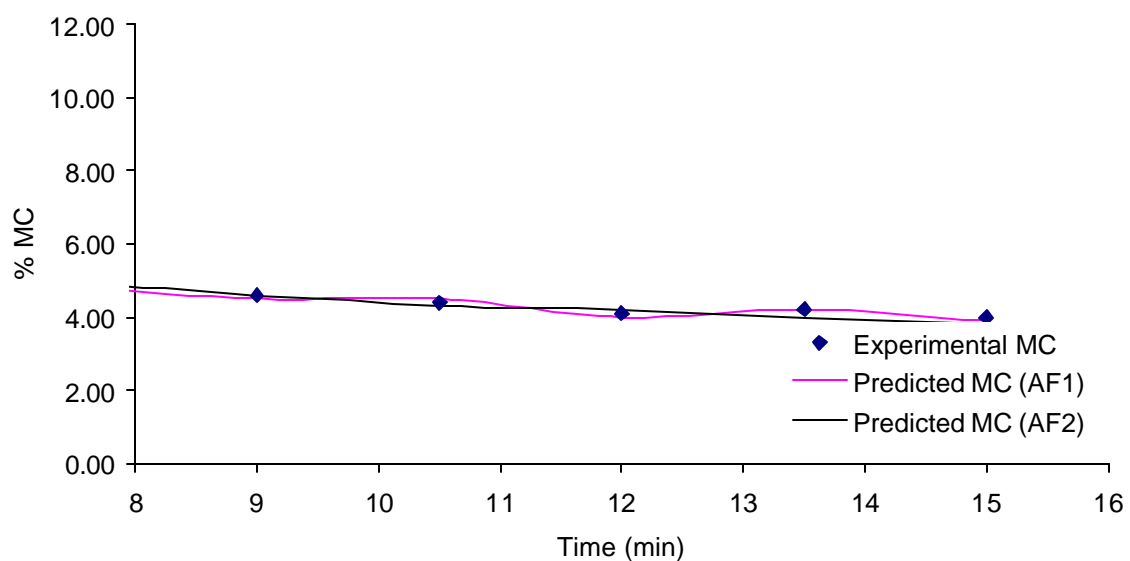


Figure V.31. Moisture content prediction for the falling rate period of the varying composition experiments at $AF=60 \text{ m}^3/\text{hr}$ and $T=60^\circ\text{C}$ (Formulation3) using correlations AF1 and AF2

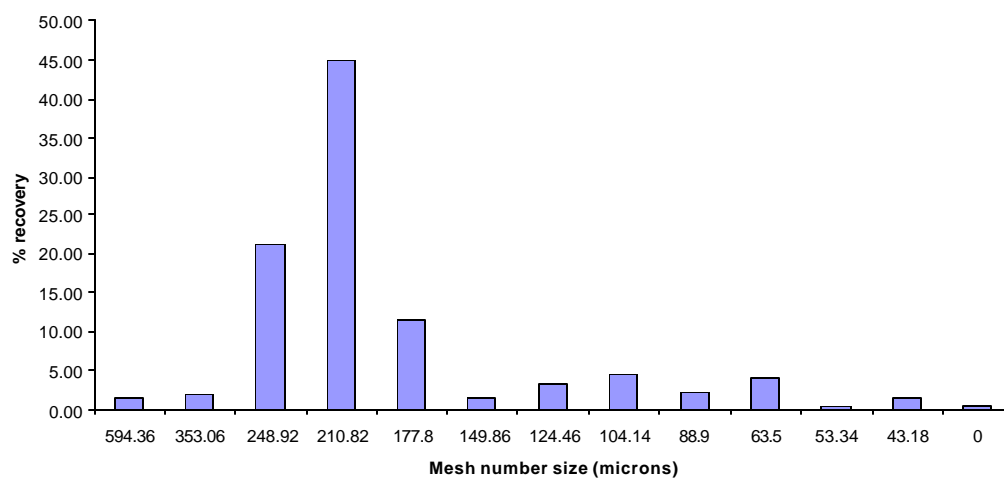


Figure V.32. Particle size distribution for granulation

VI. CONCLUSIONS AND RECOMENDATIONS

VI.1 Conclusions

An excellent prediction for the final moisture content for pharmaceutical powders using empirical correlation for the $k_g a$ was obtained.

The drying curves obtained in this investigation showed the influence of the air flow and the drying temperature in the process. The prediction of MC curves of some pharmaceutical powders in a FBD can be achieved by correlating $k_g a$ with just air flow velocity and drying temperature.

The obtained drying curves demonstrate that in the constant rate period the evaporation rate does depend on the air conditions and is independent of the solid. For the falling rate period, the controlling process was the diffusion of moisture, which is dependent on the internal drying factors.

The drying curves generated during the analysis show a non-linear behavior. It is evident that an increase of the air flow in the fluid bed dryer accelerates the drying of the particles within the granulation. The existence of the constant and falling rate periods is evident as well, while the air flow increase and a competition for the controlling step appears. Therefore it can be concluded that the moisture content behavior in the drying curves is not linear.

The predicted values of the $k_g a$ obtained from the correlations had in general a mean error of 10%, which is below the suggested threshold of 30%.

The dimensionless groups chosen to correlate the $k_g a$, contain critical parameters (air velocity and temperature) that are sufficient to describe the drying process in a FBD. The Sc number was a strong influenced by temperature in the same way that Re number showed dependence on the air flow velocity. Also, it was found that the Sc number decreases with a high value of AF and with high T ranges. The obtained results for the Sh number showed the dependency on both parameters (T and AF).

For this investigation, Re was strongly influenced by air flow. This performance was achieved due to the highest c number of the empirical parameters. Chen *et. al.* found similar results.

The final moisture content prediction resulted within the established parameter of the industry (less than 1%). The obtained absolute average residual result was 0.18. Therefore is indicates that the correlation can be used to predict the final moisture content on pharmaceutical powders within the established range of Re and Sc .

The obtained results in the prediction using only these factors, demonstrate that other factors such as porosity, particle size, and varying the composition of the granulation do not have a strong influence in the prediction of MC for the granulation used.

It can be concluded that the empirical correlation developed in this research could be used with similar pharmaceutical powders and same operating conditions with a Re range of 0.45×10^5 to 3.50×10^5 and a Sc range of 0.7-0.8.

In this research the most significant contribution compared to previous works is in terms of the prediction of the final moisture content using controllable parameters such as temperature (T) and air flow (AF). Also the great influence of the mass transfer

coefficient ($k_g a$) in the drying process was established in order to perform the prediction using the correlation. Other correlations in previous works involve difficult parameters to control such as the relative humidity, diffusivity, density, particle size, and porosity, but did not consider the mass transfer coefficient.

Another contribution of this research consists in the investigation of the different periods (constant and falling rate periods) that occur during the drying process. The different stages found for the drying process established the fact that the analysis was divided in two parts to make the analysis. Other investigators developed empirical correlations without considering the different periods. The values predicted by the correlation compare significantly with the experimental LOD results demonstrating the validity of the analysis.

VI.2 Recommendations

Future efforts:

- To improve the empirical correlation it is recommended to use values between the used operating conditions for example AF 45, 55, and 65 m³/hr, and others to increment the operational range.
- To validate the empirical correlation using different pharmaceutical powders such as corn starch, lactose, microcellulose, magnesium stearate and other with similar chemistry characteristics to expand the ranges of correlations.
- Develop an empirical correlation at the same operating conditions with other humidity techniques such as NIR.
- Use the developed empirical correlation in an industrial dryer and adjust the parameters to scale up.
- To validate the empirical correlation using an active ingredients.

LITERATURE CITED

- Alden, M., P Torkington, and A.C.R. Strutt, "Control and instrumentation of a Fluid Bed Dryer using Temperature Difference Technique: *I*. Development of a working model" *Powder Technology*, **54**, pp 15-25, (1988).
- Bennett, C.O., and J.E. Myers, "*Momentum, Heat and Mass Transfer.*" McGraw Hill Chem. Eng. Series, Third ed., New York, US, pp 550, 648-654, (1982).
- Bird, R.B., W.E. Stewart, and E.N. Lightfoot, "*Transport Phenomena.*" J. Wiley & Sons, New York, U.S., Second ed., pp 525-529, 861-866, (2002).
- Chen G.F., W. Wang, H. Yan, and X.Z. Wang, "Experimental research on mass transfer in a Centrifugal Fluidized Bed Dryer." *Drying technology*, **14** (9), pp. 1845-1857, (1999).
- Cussler E.L. "*Diffusion mass transfer in fluid systems.*" Press Syndicate of the University of Cambridge, (1994)
- Hjertager, B.H., V. Mathiesen, and T. Solberg, "*Computational analysis of some fluidized systems.*" AIChE Symposium Series, **321** (95), pp. 1-6, (1999).
- Kneule F., "*El Secado.*" Ediciones Urmo, Espartero, 10 Bilbao, pp 101-124, 152-174 (1966).
- Lipták, B., "Optimizing Dryer Performance Through Better Control" *Chem. Eng. Prog.*, February, pp. 110-114, (1998).
- Montgomery D.C., "*Design and analysis of experiments*", J. Wiley & Sons, New York, U.S., Five ed., pp 573-583, (1996).
- Mikami, T., H. Kamiya, and M. Horio, "Numerical simulation of cohesive powder behavior in a fluidized bed." *Chem. Eng. Sc.*, **10** (53), pp. 1927-1940, (1998).
- Oldshue J.Y., "*Fluid Mixing Technology.*" McGraw Hill Chem. Eng. Series, pp 233-241, (1989).
- Robinson, J.W., "Improve dryer control" *Chem.Eng. Prog.*, pp. 28-33, (1992).
- Seibert K.D., and M.A. Burns, "*Simulation of fluidized beds and other fluid-particle systems using statistical mechanic.*" AIChE Journal, **3** (42), pp. 660-670, (1996).
- Shinskey F.G., "*Process Control Systems.*" McGraw Hill Chem. Eng. Series, Second ed., New York, US, pp 322-325, (1979).

Siettos C.I., C.T. Kiranousdis, and G.V. Bafas, "Advanced Control Strategies for Fluidized Bed Dryers." *Drying Technology*, **17** (10), pp. 2271-2291, (1999).

Smith, J.M., H.C. Van Ness, and M.M. Abbot, "*Introduction of Chemical Engineering Thermodynamics*." McGraw Hill Chem. Eng. Series, Five ed., pp 55, 450-489, (1987).

Treybal R.E., "*Mass Transfer Operations*." McGraw Hill Chem. Eng. Series, pp 63, 576-599, (1978).

Wang, Z. H., and G. Chen, "Heat and mass transfer during low intensity convection drying." *Chem. Eng. Sc.* **54**, pp. 3899-3908, (1999).

Wang, Z.H. and G. Chen, "Heat and mass transfer in batch fluidized-bed of porous particles." *Chem. Eng. Sc.*, **55**, pp. 1857-1869, (2000).

Vojtěch V., and R. Drbohlav, "*Fluidized Bed Drying*" Chemical and Process Engineering Series, pp 17-81, (1966).

APPENDIX

A. Results of $k_g a$ prediction

Table A.1. Results of prediction for constant rate period for AF1

	Sc	Sh	Re	$k_g a$ cm/s	$k_g a$ (pred) cm/s	% error
AF 40 T60	0.754	33.784	7.505E+04	0.780	0.691	12.879
AF 40 T80	0.707	24.238	7.071E+04	0.597	0.775	22.968
AF 50 T60	0.758	56.017	9.440E+04	1.285	1.144	12.325
AF 50 T80	0.707	52.889	8.850E+04	1.300	1.292	0.619
AF 60 T60	0.773	69.950	1.151E+05	1.569	1.668	5.935
AF 60 T80	0.712	81.432	1.073E+05	1.979	1.942	1.905

Table A.2. Results of prediction for falling rate period for AF1

	Sc	Sh	Re	$k_g a$ cm/s	$k_g a$ (pred) cm/s	% error
AF 40 T60	0.784	4.033	7.424E+04	0.094	0.107	13.141
AF 40 T80	0.726	4.470	6.952E+04	0.113	0.118	4.426
AF 50 T60	0.774	5.753	9.335E+04	0.135	0.135	0.000
AF 50 T80	0.717	6.307	8.734E+04	0.159	0.149	6.367
AF 60 T60	0.751	7.294	1.129E+05	0.170	0.167	1.498
AF 60 T80	0.713	6.832	1.046E+05	0.173	0.179	3.509

Table A.3. Results of prediction for constant rate period for AF2

	Sc	Sh	Re	$k_g a$ cm/s	$k_g a$ (pred) cm/s	% error
AF 60 T60	0.782	30.514	9.642E+04	0.686	0.731	6.559
AF 60 T80	0.719	30.888	8.950E+04	0.755	0.874	15.762
AF 70 T60	0.776	40.153	1.121E+05	0.910	0.915	0.549
AF 70 T80	0.722	29.759	1.013E+05	0.722	1.011	40.028
AF 80 T60	0.769	45.391	1.150E+05	1.033	0.982	4.937
AF 80 T80	0.721	56.309	9.620E+04	1.354	0.941	30.502

Table A.4. Results of prediction for falling rate period of AF2

	Sc	Sh	Re	$k_g a$ cm/s	$k_g a$ (pred) cm/s	% error
AF 60 T60	0.795	8.753	1.14E+05	0.202	0.207	2.475
AF 60 T80	0.730	7.677	1.06E+05	0.192	0.198	3.125
AF 70 T60	0.795	11.474	1.33E+05	0.264	0.259	1.893
AF 70 T80	0.730	10.213	1.24E+05	0.255	0.247	3.137
AF 80 T60	0.789	12.111	1.41E+05	0.279	0.281	0.717
AF 80 T80	0.723	11.889	1.42E+05	0.297	0.300	1.010

B. Polymath output to determine the parameters for the empirical correlation

Constant rate period (AF1)

POLYMATH Results

Nonlinear regression (L-M)

Model: $Sh = A(Sc^b)(Re^c)$

Variable	Initial guess	Value	95% confidence
A	0.002	1.023E-10	8.633E-10
b	-3	-2.8266514	3.8695707
c	3	2.2810556	0.6954829

NOTE: Calculations exceeded the maximum number of iterations.

Nonlinear regression settings

Max # iterations = 64

Precision

$R^2 = 0.944707$

$R^2_{adj} = 0.907845$

Rmsd = 1.8800641

Variance = 42.415694

General

Sample size = 6

Model vars = 3

Indep vars = 2

Iterations = 64

Falling rate period (AF1)

POLYMATH Results
Nonlinear regression (L-M)

Model: $Sh = A \cdot (Sc^b) \cdot (Re^c)$

Variable	Initial guess	Value	95% confidence
A	5.0E-04	7.131E-05	1.644E-04
b	-1	-1.1105649	2.4673246
c	0.8	0.9627194	0.1981432

NOTE: Calculations exceeded the maximum number of iterations.

Nonlinear regression settings
Max # iterations = 64

Precision

$R^2 = 0.9179165$
 $R^2_{adj} = 0.8631942$
 $Rmsd = 0.1387551$
 $Variance = 0.2310356$

General

Sample size = 6
 # Model vars = 3
 # Indep vars = 2
 # Iterations = 64

POLYMATH 5.0 Results
Nonlinear regression (L-M)

Model: $Sh = A \cdot (Sc^b) \cdot (Re^c)$

Nonlinear regression settings
Max # iterations = 64

Precision

$R^2 = 0.1686459$
 $R^2_{adj} = -0.3855901$
 $Rmsd = 3.6116336$
 $Variance = 156.52677$

General

Sample size = 6

Model vars = 3

Indep vars = 2

Iterations = 64

Falling rate period (AF2)

POLYMATH Results

Nonlinear regression (L-M)

Model: $Sh = A \cdot (Sc^b) \cdot (Re^c)$

Variable	Initial guess	Value	95% confidence
A	5.0E-04	5.617E-07	1.283E-06
b	0.05	0.295482	0.8623022
c	0.9	1.4308661	0.1921365

NOTE: Calculations exceeded the maximum number of iterations.

Nonlinear regression settings

Max # iterations = 64

Precision

 $R^2 = 0.9833508$ $R^2_{adj} = 0.9722513$

Rmsd = 0.0872106

Variance = 0.0912683

General

Sample size = 6

Model vars = 3

Indep vars = 2

Iterations = 64

C. Prediction of MC for falling rate period (AF1)

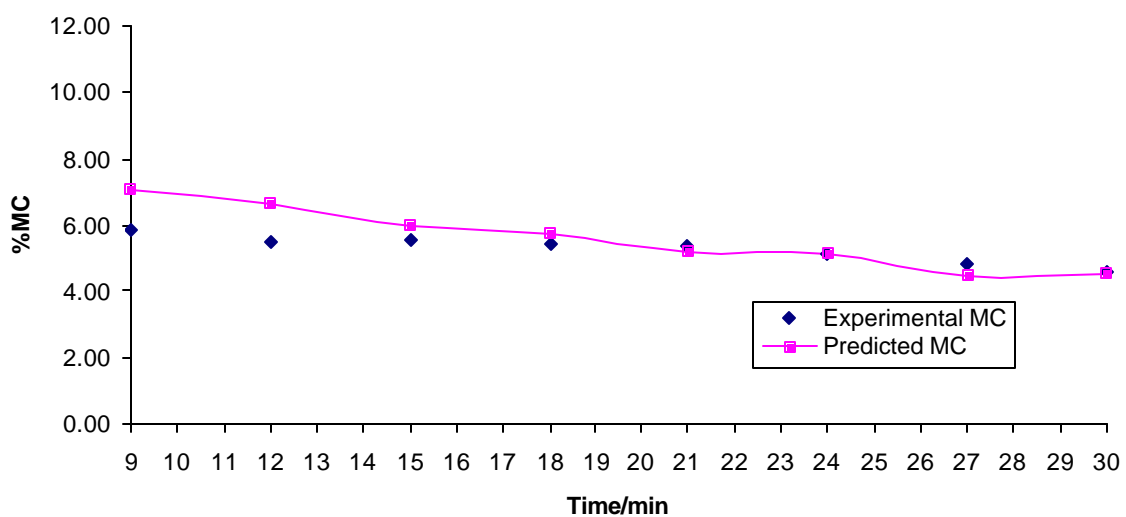


Figure C.1. Diagram of moisture content for falling rate period for AF 50 m³/hr and T=80 °C

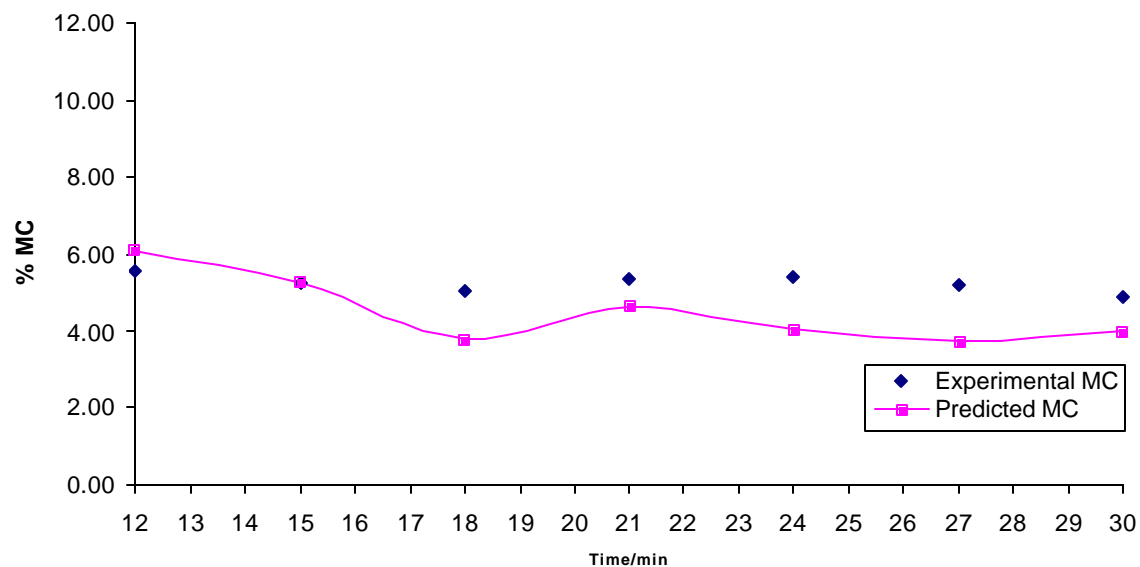


Figure C.2. Diagram of moisture content for falling rate period for of AF 50 m³/hr and T=60 °C

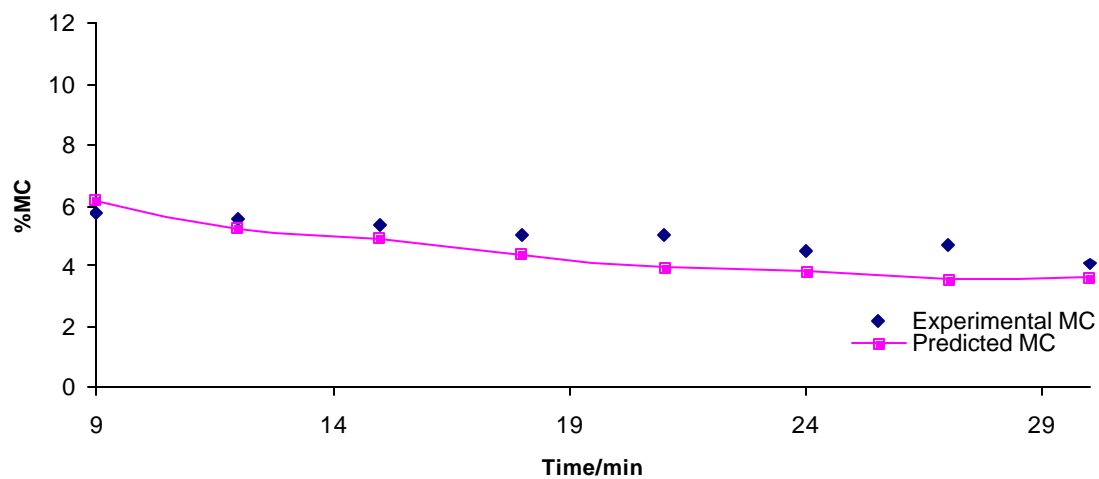


Figure C.3. Diagram of moisture content for falling rate period for AF 60 m³/hr and T=80 °C (AF1)

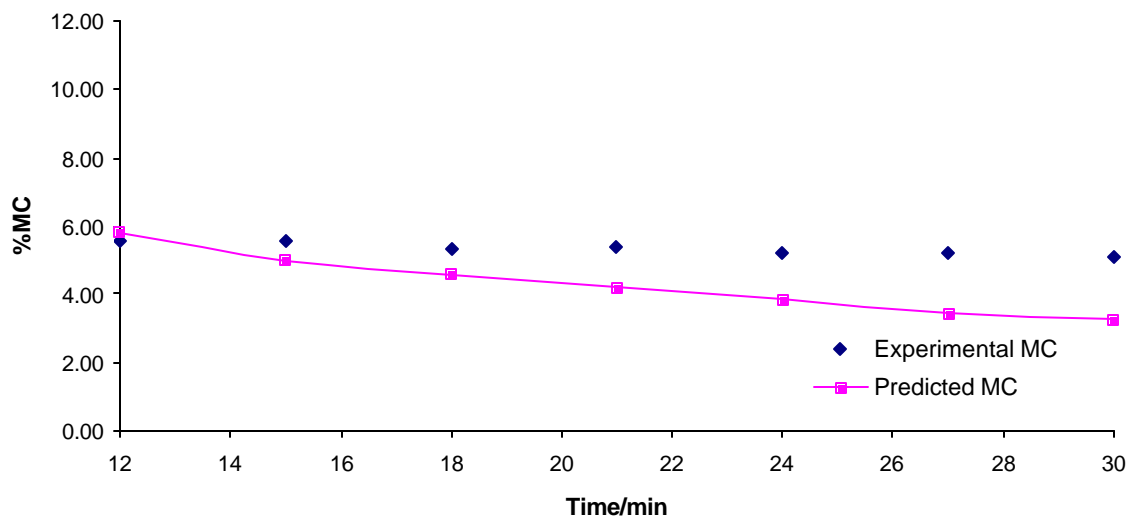


Figure C.4. Diagram of moisture content for falling rate period for AF 60 m³/hr and T=60 °C

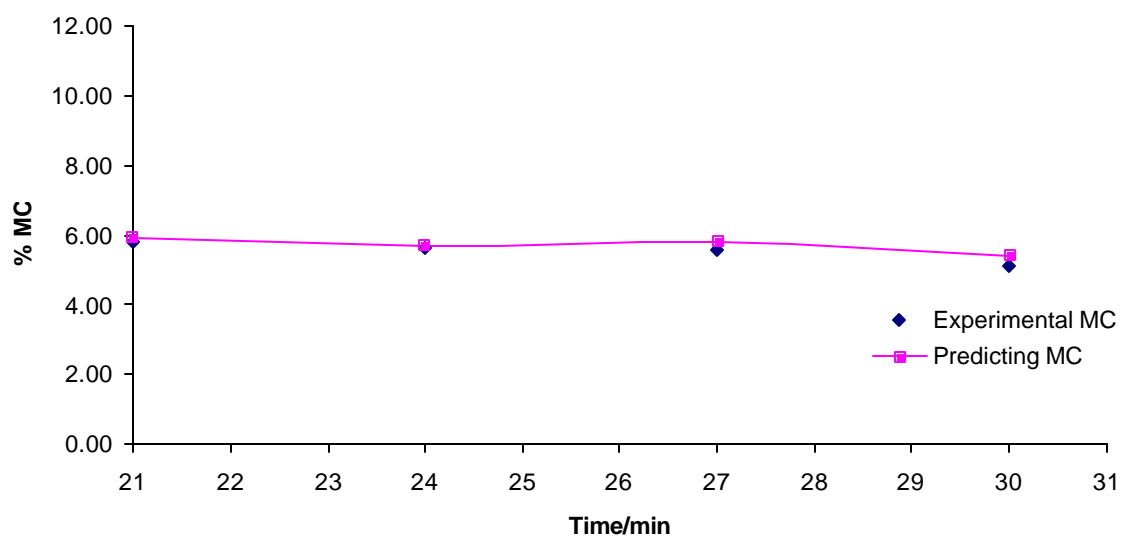


Figure C.5. Diagram of moisture content for falling rate period for AF 40 m³/hr and T=80 °C

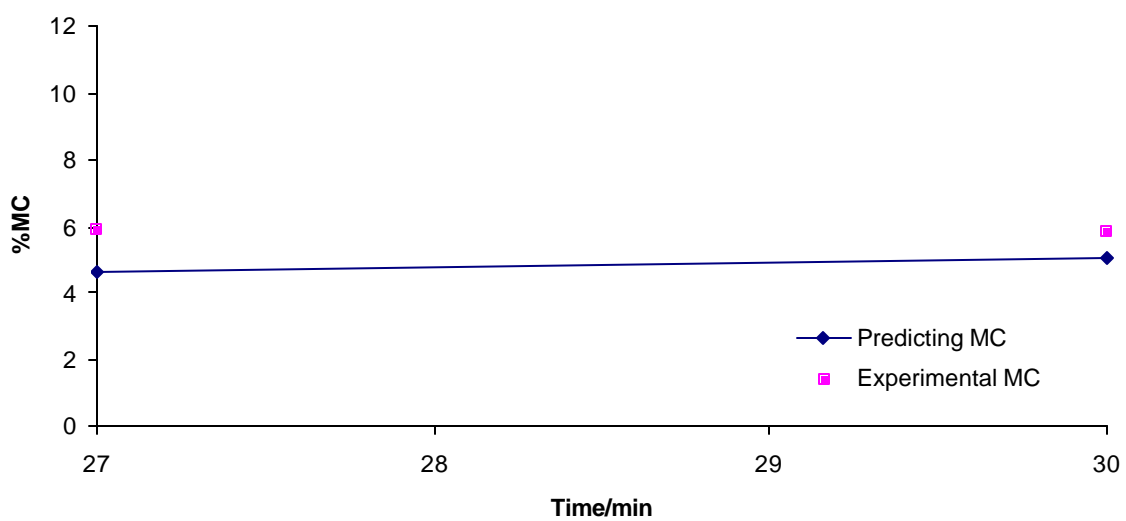


Figure C.6. Diagram of moisture content for falling rate period for AF 40 m³/hr and T=60 °C

D. Prediction of MC for constant rate period (AF2)

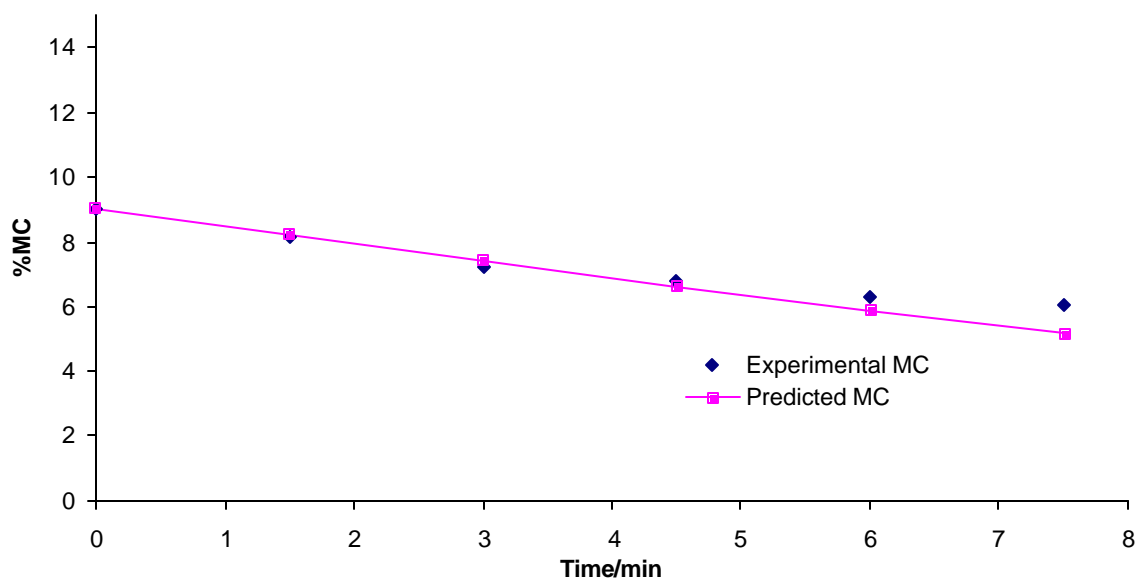


Figure D.1. Diagram of moisture content for constant rate period for AF 60 m³/hr and T=80 °C (AF2)

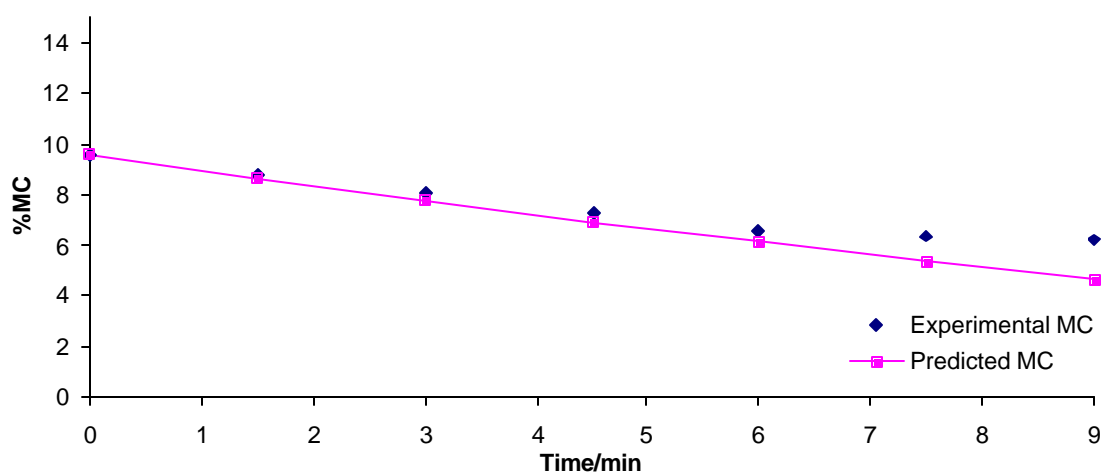


Figure D.2 Diagram of moisture content for constant rate period for AF 60 m³/hr and T=60 °C (AF2)

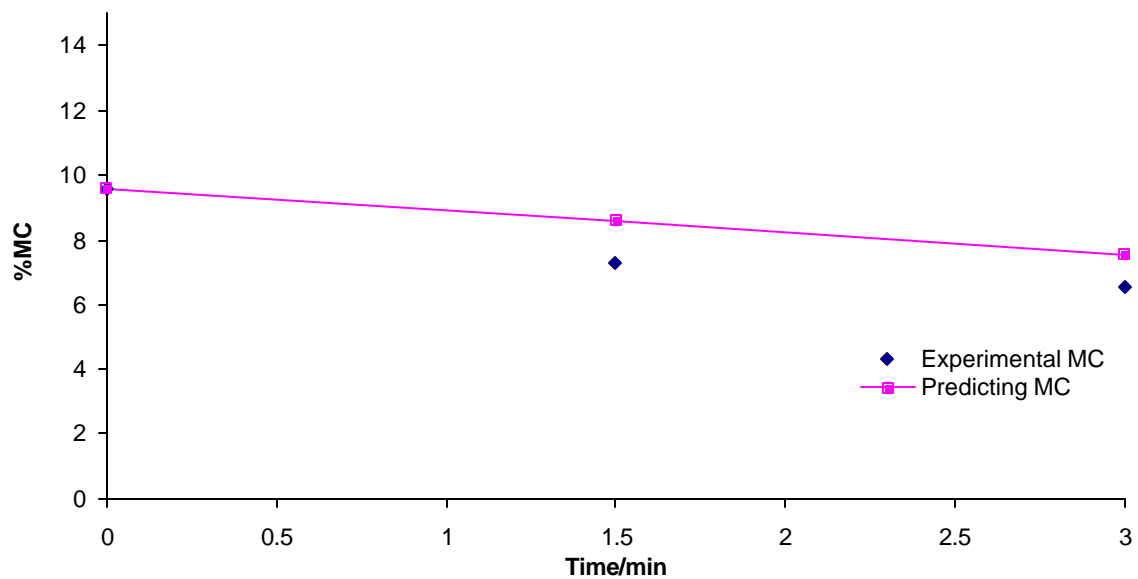


Figure D.3. Diagram of moisture content for constant rate period for AF 80 m³/hr and T=80 °C

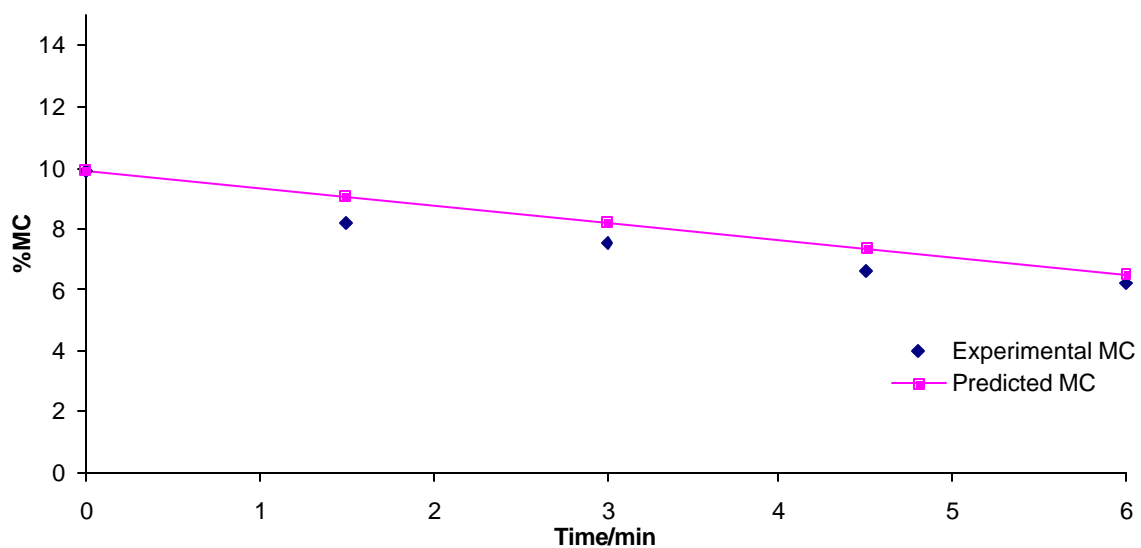


Figure D.4. Diagram of moisture content for constant rate period for AF 80 m³/hr and T=60 °C

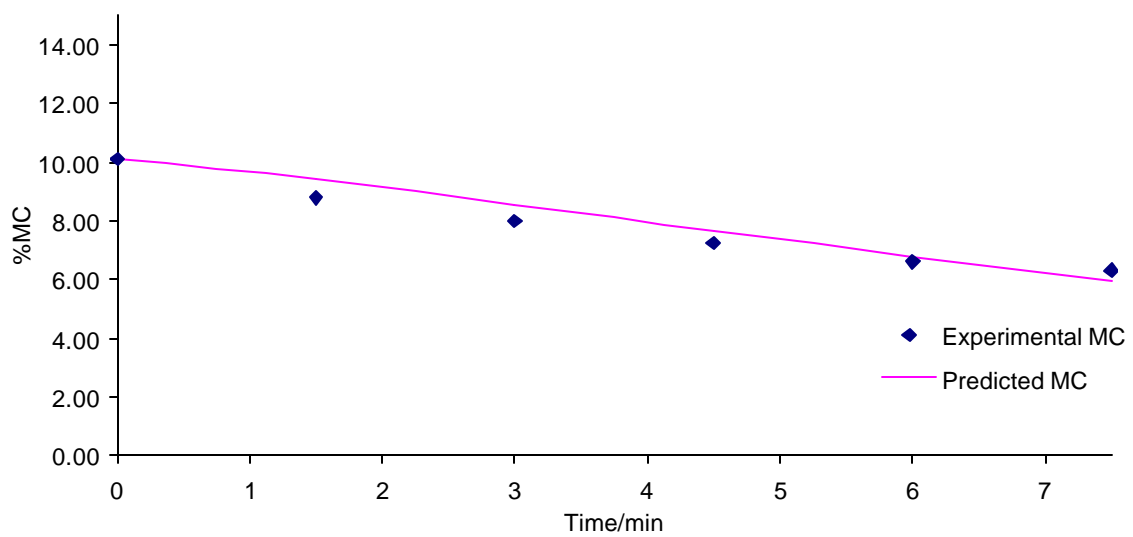


Figure D.5. Diagram of moisture content for constant rate period for AF 70 m³/hr and T=60 °C

E. Prediction of MC for falling rate period (AF2)

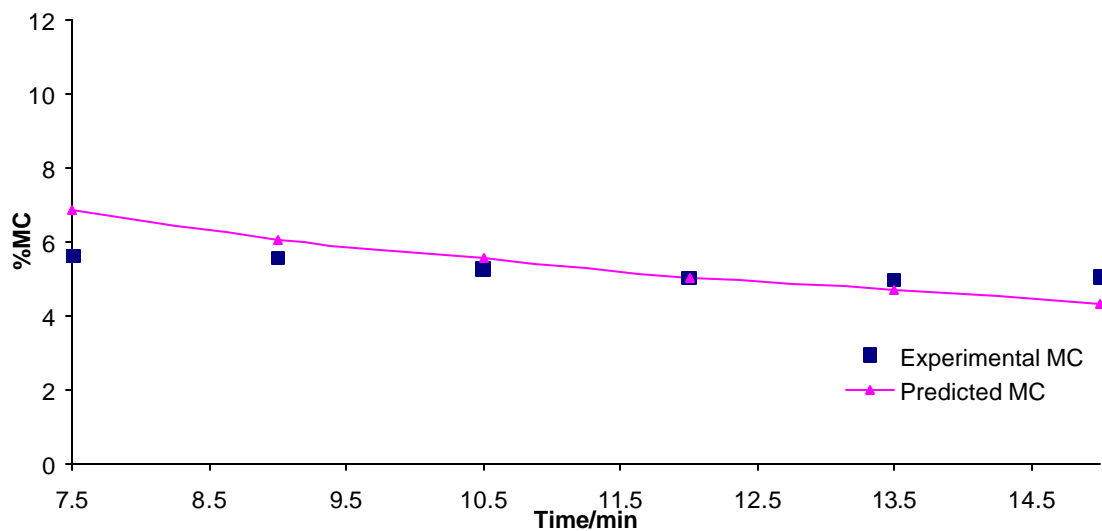


Figure E.1. Diagram of moisture content for falling rate period for AF 70 m³/hr and T=80 °C

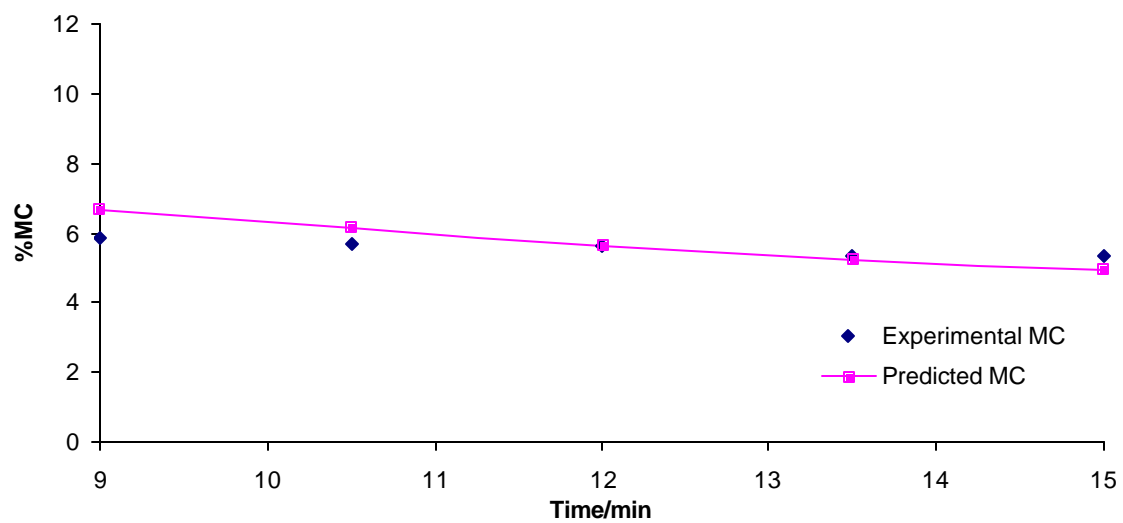


Figure E.2. Diagram of moisture content for falling rate period for AF 70 m³/hr and T=60 °C

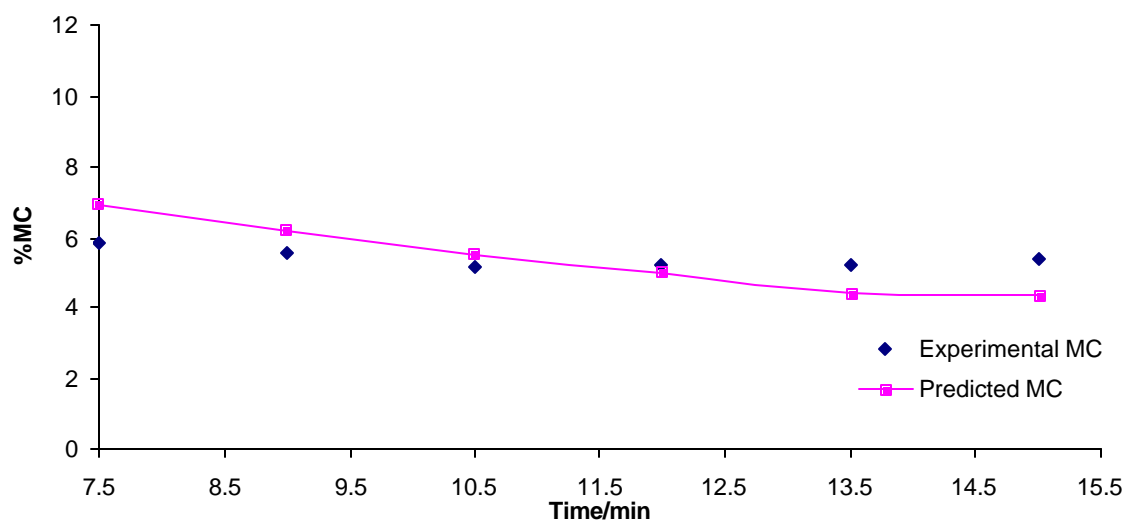


Figure E.3. Diagram of moisture content for falling rate period for AF 80 T60

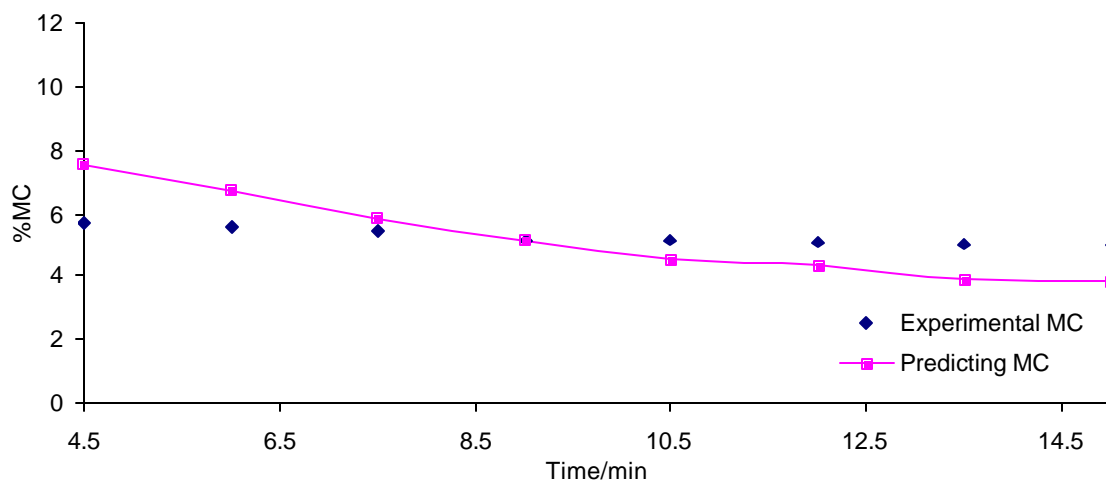


Figure E.4. Diagram of moisture content for falling rate period for AF 80 m³/hr and T=80 °C

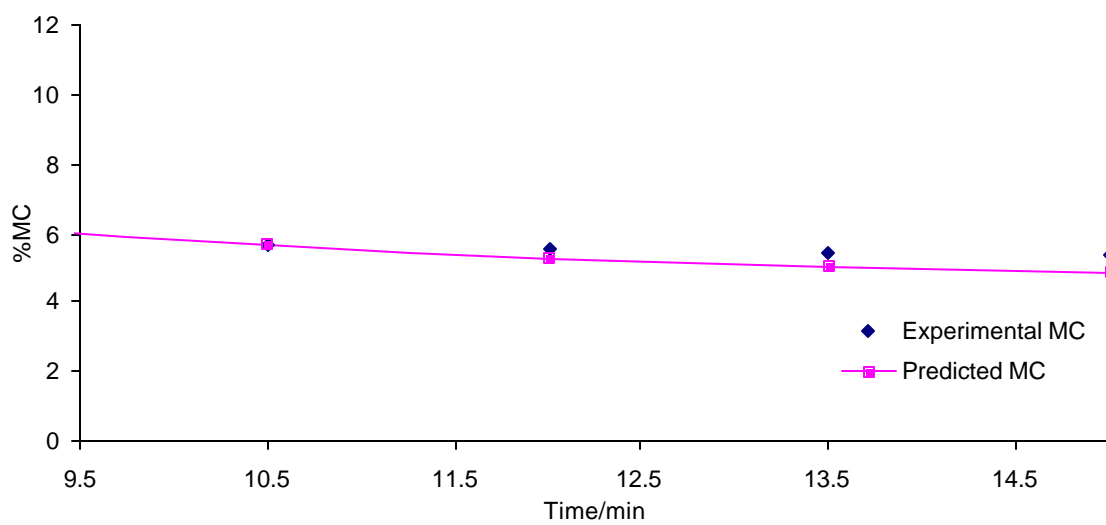


Figure E.5. Diagram of moisture content for falling rate period for AF 60 m³/hr and T=80 °C (AF2)

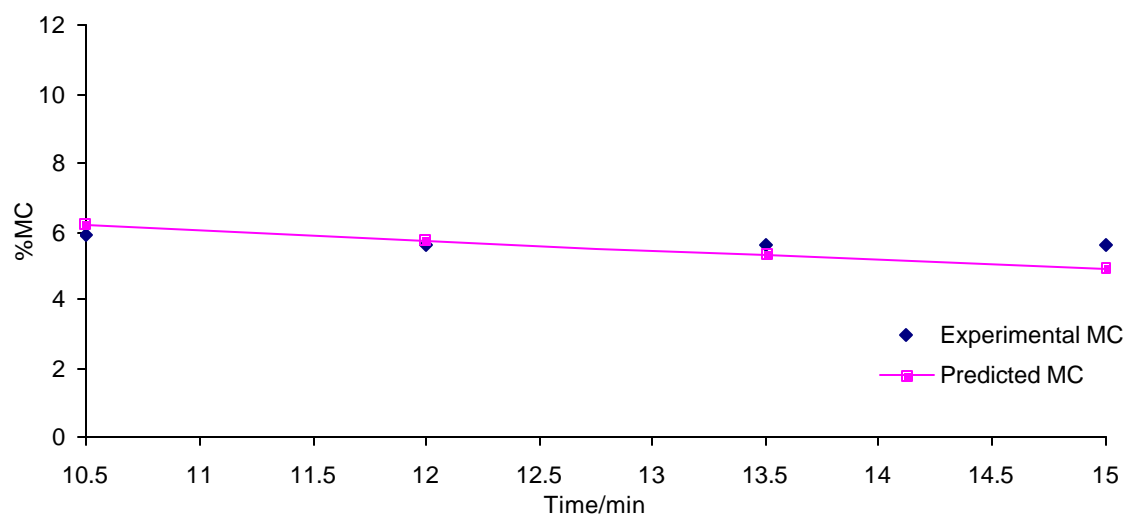


Figure E.6. Diagram of moisture content for falling rate period for AF 60 m³/hr and T=60 °C